

Quasi-Optical Multi-Beam Antenna Technologies for B5G and 6G mmWave and THz Networks: A Review

Y. JAY GUO¹ (Fellow, IEEE), MARAL ANSARI¹ (Student Member, IEEE),
RICHARD W. ZIOLKOWSKI¹ (Life Fellow, IEEE),
AND NELSON J. G. FONSECA² (Senior Member, IEEE)

(Invited Paper)

¹Global Big Data Technologies Centre, University of Technology Sydney, Ultimo, NSW 2007, Australia

²Antenna and Sub-Millimetre Waves Section, European Space Agency, 2200 AG Noordwijk, The Netherlands

CORRESPONDING AUTHOR: Y. J. GUO (e-mail: jay.guo@uts.edu.au)

ABSTRACT Multi-beam antennas are critical components in future terrestrial and non-terrestrial wireless communications networks. The multiple beams produced by these antennas will enable dynamic interconnection of various terrestrial, airborne and space-borne network nodes. As the operating frequency increases to the high millimeter wave (mmWave) and terahertz (THz) bands for beyond 5G (B5G) and sixth-generation (6G) systems, quasi-optical techniques are expected to become dominant in the design of high gain multi-beam antennas. This paper presents a timely overview of the mainstream quasi-optical techniques employed in current and future multi-beam antennas. Their operating principles and design techniques along with those of various quasi-optical beamformers are presented. These include both conventional and advanced lens and reflector based configurations to realize high gain multiple beams at low cost and in small form factors. New research challenges and industry trends in the field, such as planar lenses based on transformation optics and metasurface-based transmitarrays, are discussed to foster further innovations in the microwave and antenna research community.

INDEX TERMS Beamformers, beyond 5G (B5G), Internet in space, millimeter wave (mmWave), multi-beam antennas, quasi-optical techniques, sixth-generation (6G), terahertz (THz).

I. INTRODUCTION

THE FIFTH-GENERATION (5G) mobile and wireless systems are posing challenges to the already congested microwave frequency spectrum with their promise to support high data rates and to achieve low latency. These systems are separated into two categories: Frequency Range 1 (FR1), which includes all frequency bands below 6 GHz, and Frequency Range 2 (FR2), which covers the so-called 5G millimeter wave (mmWave) bands currently being trailed around the world to address these challenges. It is expected that various parts of the lower mmWave spectrum, <50 GHz, will be gradually subjugated by 5G systems in the coming decade. However, the data rates are expected to be much higher, on the order of terabits per second (Tbps), as wireless technologies evolve into sixth-generation (6G) systems. This advance will pose even more challenges to the already scarce

radio spectrum [1], [2]. There are probably only two viable solutions to address them: 1) move up to yet higher frequency bands, i.e., all the way up to terahertz (THz) frequencies; or 2) implement dynamic spectrum sharing and abandon the fixed spectrum allocation paradigm. Future systems will most likely include a combination of these two solutions. This paper is focused primarily on technologies being developed for solution 1. Owing to their small physical antenna sizes, the higher frequency band solutions also serve as one of the most promising technologies for space-borne and airborne platforms, i.e., Internet in space (space-Internet) systems as well as integrated terrestrial and non-terrestrial networks in general [3], [4].

Similar to their lower frequency counterparts, these high frequency mmWave and THz antennas must produce multiple beams in order to support dynamic networking and

to realize long range communications. Because the wavelengths at mmWave and THz frequencies are physically small, these antenna systems generally have a quasi-optical nature. Therefore, the associated beamforming devices, in contrast to the standard circuit type beamforming networks associated with lower frequency multi-beam antennas [5], need to be designed primarily based on optical theory and principles, as described in [6]. Furthermore, mmWave and THz fields propagate in a pseudo-light fashion and, hence, their interactions with mobile platforms are highly localized.

The concept of quasi-optical antenna design is not new as early high gain microwave antennas were mainly lenses and reflectors directly derived from their optical counterparts. Nevertheless, while quasi-optical 6G and space-Internet antennas have obvious advantages, they pose many practical issues. Since their operating wavelengths are small, they can be easily fit into a physically small platform achieving compactness, low weight and low cost. On the other hand, fabricating and measuring quasi-optical 6G and space-Internet antennas are arguably more demanding because they are very small. New technologies, materials and processes will need to be developed.

In this paper, we provide a comprehensive review of various quasi-optical beamformers and multi-beam antennas suitable for beyond 5G (B5G) and more specifically 6G systems for the first time. This paper is organized as follows. First, the detailed analysis and design of different lens-based beamformers and multi-beam antennas for mmWave operations are given. These lenses include the classical Ruze, Rotman, and Luneburg designs. Moreover, nonclassical planar lenses based on transformation optics (TO) and metamaterials are also reviewed and discussed. Second, reflector-based beamformers for realizing multi-beam antennas at mmWave frequencies are presented. Third, recent developments of lens-based THz antennas are described. Finally, the latest technological developments and research challenges for quasi-optical beamformers are reported.

II. MULTIPLE BEAM ANTENNAS BASED ON CLASSICAL LENSES

Lenses are well-known structures used to collimate the electromagnetic waves radiated from a source. A lens was used with a radio antenna as early as in 1889 by Lodge and Howard [7]. In the same way as in optics, a microwave lens can be used to create directive radiation from a point source or conversely receive the energy of a plane wave and concentrate it at its focal point. A lens is often used in combination with other aperture antennas such as horns or reflectors [8]. The primary purpose of using a lens structure in most applications is to increase the gain of the antenna by transforming a spherical wavefront into a planar one. As with any type of aperture-based antenna, the aperture size relative to the operational wavelength is directly correlated to the maximum directivity that a lens antenna can produce and the absolute maximum is attained if the entire aperture is uniformly illuminated.

In contrast to reflectors, lenses have no aperture blockage caused by their feeds. Nevertheless, they may incur internal and surface-reflection losses, and they must be edge-supported which can lead to scattering losses. In comparison to reflectors, lenses have generally more degrees of freedom to shape their output wavefront. These include the shapes of their inner and outer surfaces, as well as the distribution of the effective refractive index in them or some other characteristic that alters the propagation of electromagnetic waves through them.

The concept of employing lenses to produce multi-beam antennas initially emerged in the late 1940s and early 1950s [9], mostly targeting radar applications. Nevertheless, its serious commercial exploitation has only happened in recent years with the extreme growth of mmWave applications for which the size and weight of typical lens solutions become acceptable. The renewed interest in lenses is also linked to the recent development of artificial dielectrics and other metamaterial constructs [10]–[14].

Detailed design principles and various examples of different types of lens-based beamformers are reviewed in this section. These will include the conventional Ruze, Rotman, and Luneburg lenses. New research challenges to advance the state of the art of lenses are discussed.

A. RUZE LENS

Ruze reported a 2D lens theory in his seminal paper [15] to realize multiple beams with greater beam coverage. A Ruze lens consists of metal parallel plates that are capable of constraining the electromagnetic energy to travel parallel to the axis of the lens with a phase velocity that differs from that in free space. It is a particular implementation of the so-called “constrained” or “path-length” lenses, in which the rays do not obey Snell’s law.

Traditional lenses typically have only one focal point. Ruze proposed employing an elliptical lens with two or three focal points and multiple feed locations along the focal arc to produce the desired multiple beams.

As illustrated in Fig. 1(a), the points O_1 and O_2 are the focal points of two beams symmetrically radiated in the x - y plane. These beams are denoted as beam 1 and beam 2. They are directed at the angles $\pm\alpha$, which are equal to the feed offset angles. The electric field is polarized parallel to the z -axis in order to control its phase velocity, while the metal-plates forming the lens are normal to the y -axis. The following development, reported to illustrate a method used to design constrained lenses, corresponds to the particular case of a lens with constant thickness. A more general development can be found in [15].

The element phase compensation for beam 1 must satisfy the relation:

$$k_0 l_1 - \phi_{r1}(x, y) = k_0(l_0 + x \cos \alpha + y \sin \alpha) - \phi_{r1}(0, 0) \quad (1)$$

where l_1 represents the distance between the focal point and a position (x, y) on the inner lens contour; l_0 represents the distance between that same focal point and the center of the

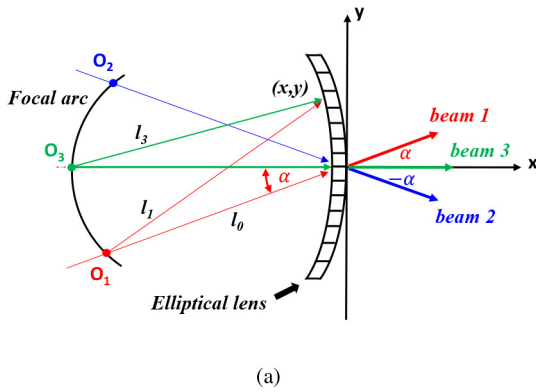


FIGURE 1. Schematic representation of a Ruze lens with constant thickness. (a) Elliptical section. (b) Corresponding straight section.

lens, referred to as focal length; and k_0 is the wavenumber in free space. The element phase compensation value at the point (x, y) is $\phi_{t1}(x, y)$. It is $\phi_{t1}(0, 0)$ at $(0, 0)$. The distance l_1 is calculated with geometric considerations.

Defining U as:

$$U = \frac{\Delta\phi_{t1}}{k_0} = \frac{\phi_{t1}(x, y) - \phi_{t1}(0, 0)}{k_0} \quad (2)$$

one obtains after some manipulations:

$$\begin{aligned} x^2 \sin^2 \alpha + y^2 \cos^2 \alpha - 2xy \sin \alpha \cos \alpha \\ = u^2 + 2ul_0 + 2uy \sin \alpha + 2ux \cos \alpha \end{aligned} \quad (3)$$

Similarly, considering the focal point at O_2 for beam 2 with the angle $-\alpha$, one also has:

$$\begin{aligned} x^2 \sin^2 \alpha + y^2 \cos^2 \alpha + 2xy \sin \alpha \cos \alpha \\ = u^2 + 2ul_0 - 2uy \sin \alpha + 2ux \cos \alpha \end{aligned} \quad (4)$$

Combining (3) and (4), one obtains the phase compensation equation in the x - y plane along with the ideal elliptical lens contour. They are given by the expressions:

$$\Delta\phi_{t1} = k_0 u = -k_0 x \cos \alpha \quad (5)$$

$$\left(\frac{x}{l_0 \cos \alpha} + 1 \right)^2 + \left(\frac{y}{l_0} \right)^2 = 1 \quad (6)$$

where $\Delta\phi_{t1}$ represents the relative phase compensation at (x, y) with respect to the point $(0, 0)$. As can be seen from (6), the ideal inner lens contour is elliptical in the

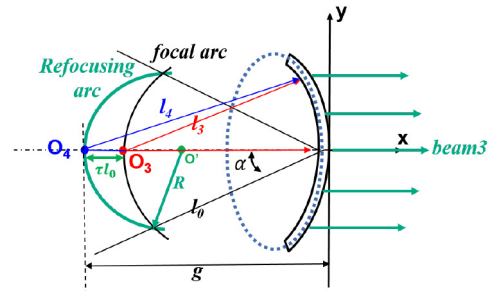


FIGURE 2. Refocusing schematic of an elliptical lens [16].

x - z plane. The phase compensation values to achieve bore-sight radiation are calculated along the straight lines shown in Fig. 1(b).

1) REFOCUSING DESIGN

The multi-beam elliptical lens with multiple feeds was designed initially assuming that the feeds would be placed along the focal arc with radius l_0 and center $(0, 0)$ as shown in Fig. 1(a). Recall that the phase compensation values along the elliptical lens were calculated relative to those for the maximum oblique angles $\pm\alpha$ corresponding to the focal points O_1 and O_2 because the constant thickness lens can only produce two focal points. Therefore, there is a phase error when the feed is located at the center of the focal arc, the feed point O_3 , and is pointed at the center of the lens to generate the boresight beam. The phase error for this beam, labeled beam 3 in Fig. 1(a), is described below to establish how a correction for it can be made. The ideal phase compensation value for beam 3 is obtained from the derived elliptical contour of the elliptical lens aperture and the relevant form of (1) as:

$$k_0 l_3 - \phi_{t3}(x, y) = k_0(l_0 + x) - \phi_{t3}(0, 0) \quad (7)$$

where l_3 denotes the distance from the focal point O_3 to any point (x, y) on the inner contour, and l_0 is the focal length specifically at O_3 . The term $\phi_{t3}(x, y)$ is the compensating phase value of the element at (x, y) , the distance l_3 is calculated with the Pythagorean theorem. Therefore, the relative phase compensation value at O_3 is $\Delta\phi_{t3}$. The phase error at point O_3 is then δ , which can be calculated as $\Delta\phi_{t3} - \Delta\phi_{t1}$. There is a good agreement between δ and δ_1 for both; and, therefore, the approximation $\delta \approx \delta_1$ is acceptable.

To compensate for the phase error at O_3 , the feed point O_3 is moved away from the elliptical lens aperture by τl_0 to the point O_4 , as illustrated in Fig. 2. The relative phase compensation value at O_4 is $\Delta\phi_{t4}$. Now consider the relationship between x and y from (6). Employing a Taylor series expansion for the value y in δ at $(0, 0)$, one finds that the first- and third-order derivatives of δ with respect to y are both zero. Thus, δ can be approximated as the second-order term:

$$\delta \approx \delta_1 = k_0 \frac{\sin^2 \alpha}{2l_0} \times y^2 \quad (8)$$

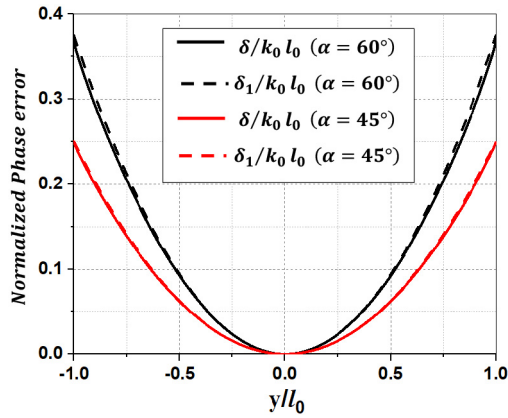


FIGURE 3. Comparison of the exact and approximated normalized phase error in a Ruze lens with constant thickness.

The corresponding plots of $\delta/k_0 l_0$ and $\delta_1/k_0 l_0$ versus y/l_0 are shown in Fig. 3 for the two cases in which the maximum beam angle α is 60° and 45° .

The phase correction resulting from this refocusing to O_4 can be obtained with $\sigma = \Delta\phi_{t4} - \Delta\phi_{t3}$ and its Taylor series expansion. One obtains:

$$\sigma \approx \sigma_1 = -k_0 \frac{1}{2l_0} \times \frac{\tau}{1 + \tau} \times y^2 \quad (9)$$

The phase aberration for the boresight beam 3 is therefore ideally fixed by refocusing the feed source to O_4 , as long as $\sigma_1 = \delta_1$. This means $\tau = \tan^2 \alpha$. A new focal arc, labeled as the refocusing arc in Fig. 2, is thus produced. Consequently, its center is moved from $(0, 0)$ to point O' , i.e., to the point $(R - g, 0)$, where $g = (1 + \tau)l_0$ is the new focal length at O_4 . The radius R is then calculated with the law of cosines. A continuous beam scan can then be realized in the range of $-\alpha$ to $+\alpha$ as the feed is rotated along the refocusing arc.

The aforementioned wide-angle scanning metal-plate lenses theory introduced by Ruze [15] is a promising research direction for the design of elliptical transmitarrays and reflectarrays. Recently, a mmWave multi-beam elliptical cylindrical transmitarray was developed for the first time. This design utilized the shape of the aperture as an additional degree of freedom. The aperture shape and the phase compensation were jointly designed according to the desired maximum beam direction, leading to different focal lengths for different beam directions. With a planar surface, the bifocal design is theoretically not possible. Nevertheless, it has been demonstrated that a pseudo-bifocal planar transmitarray can enhance scanning performance [17]. A similar bifocal approximation was also proposed to design reflectarrays [18]. Alternatively, dual-reflectarray and dual-transmitarray geometries were also considered as design techniques to enhance the scanning performance [19], [20].

Ruze lenses exhibit multiple true focal points, thus resulting in low phase aberrations over a wider scanning range. However, the port discretization resulting from the constrained lens design introduces some limitations that are

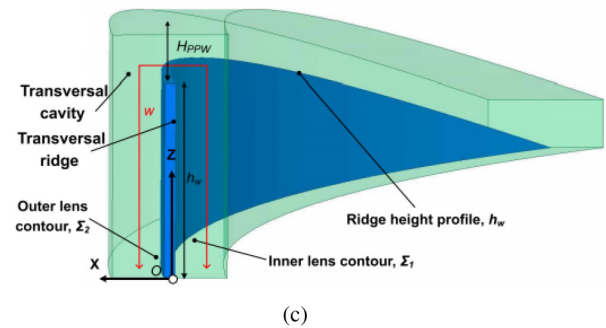
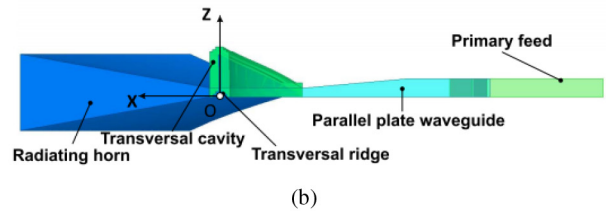
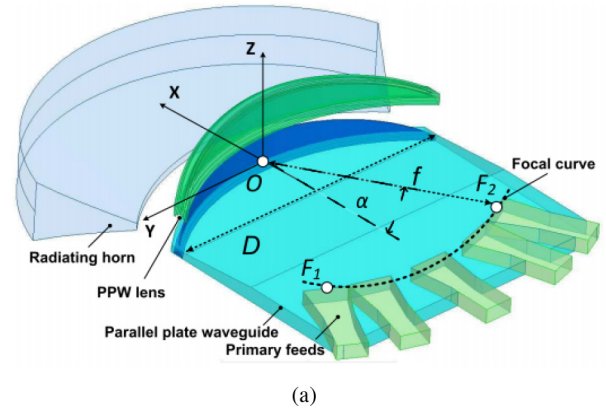


FIGURE 4. Continuous PPW lens-like beamformer. (a) 3D view. (b) Cross-sectional view in the x - z cut plane. (c) Zoomed-in view of the transversal cavity (the red line highlights the propagation path inside the transversal cavity) [21].

highly dependent on the transmission line technology used. In an attempt to overcome some of those limitations, a new concept, the continuous parallel-plate waveguide (PPW) beamformer, was introduced in [21]. This beamformer transforms the cylindrical wave, which is launched by one of the primary feeds, i.e., the sectoral horns in Fig. 4(a), and propagates inside the PPW section, into a quasi plane wave that is radiated into free space, and vice versa. The desired delay correction applied to ensure this wave transformation is provided by a PPW lens made of the transversal ridge and cavity shown in Figs. 4(b) and 4(c), whose inner and outer contours are labeled 1 and 2, respectively. Using a bifocal constrained lens approximation [22], the proposed lens design is expected to have the two focal points, F_1 and F_2 , indicated in Fig. 4(a). The associated delay value is mainly controlled by tuning the ridge height h_w , denoted in Fig. 4(c). However, this continuous design displays a residual side lobe imbalance and, thus, reveals the limitations of elliptical delay lens profiles, i.e., they do not sufficiently constrain the energy.

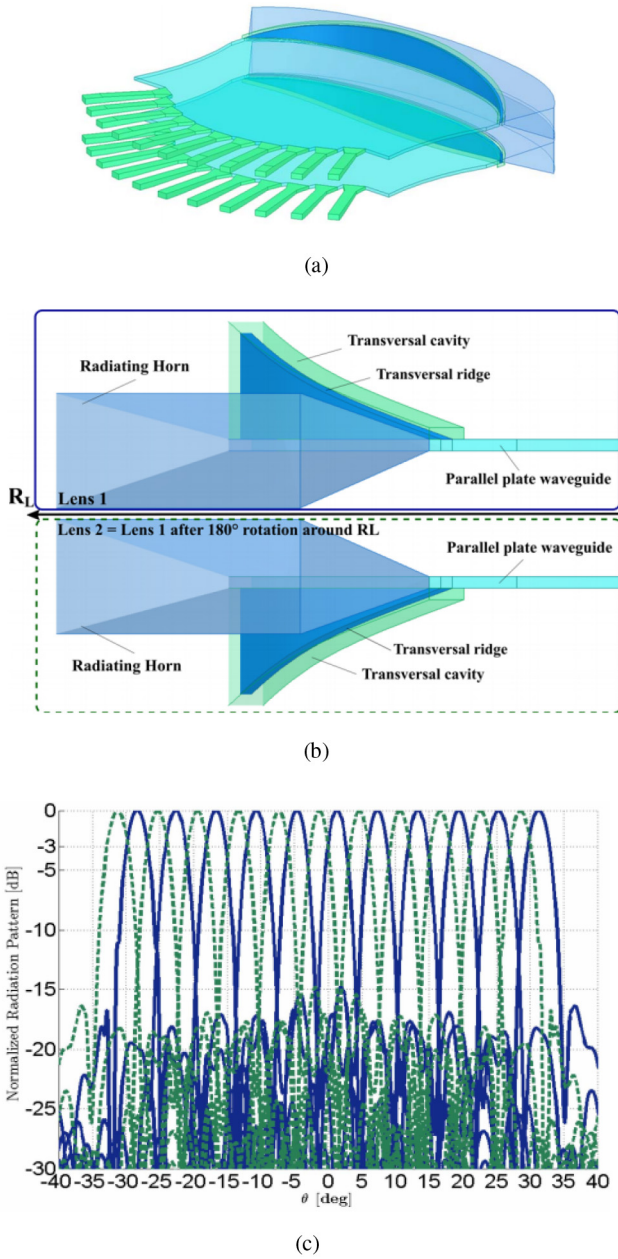


FIGURE 5. Antenna prototype. (a) Transversal blade part. (b) Transversal cavity part. (c) Measured H-plane normalized radiation patterns of the final PPW beamformer design at 30 GHz for all the feeds (continuous line) and for the same beamformer considering the 180° rotation around R_L (dashed line) [23].

To enhance the scanning performance and the pattern shape, a mmWave continuous PPW delay lens with polynomial inner/outer lens contours and ridge height profile was proposed by the authors [23]. The side view of the final configuration with Lens 2 identical to Lens 1, defined with a 180° rotation around its axis of symmetry, denoted herein as R_L , and the corresponding H-plane patterns are shown in Fig. 5. These patterns are obtained with the considered lens (continuous blue line), and they have been combined with the ones obtained after 180° rotation around R_L .

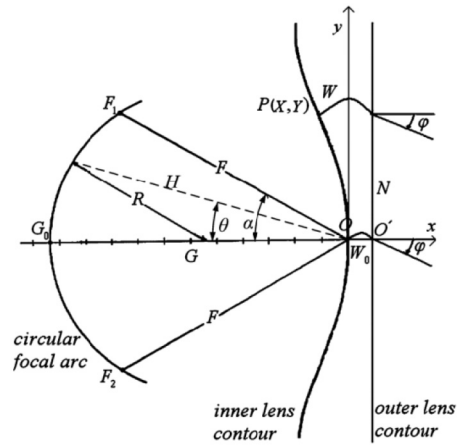


FIGURE 6. Configuration of the traditional Rotman lens [1].

B. ROTMAN LENS

The Rotman lens was introduced by Rotman and Turner in the 1960s [24]. The lens is a specific implementation of a more general form of constrained lens, also referred to as a “bootlace” lens [25]. It uses flexible transmission lines, such as coaxial lines, to connect the inner and outer lens contours. The consequent added degree of freedom enables three focal points while keeping the outer lens contour straight, thus improving the scanning performance over the equivalent Ruze lens design. Four focal points can be obtained with a curved outer lens contour [26]. Design rules follow a ray-tracing method similar to that described in the previous section, based on path length equality at the focal points.

The configuration of the traditional Rotman lens is shown in Fig. 6. It consists of a focal arc on which multiple feeds are placed. A pickup array along a separate surface is known as the “inner lens contour.” The straight line, called the “outer lens contour,” is where the antenna elements are placed. Electrical and geometrical constraints are imposed on the lens system to uniquely define its configuration: a straight front face, two symmetrical off-axis focal points F_1 and F_2 , and an on-axis focal point G_0 . These three focal points determine the fields that are radiated into the angles: $-\alpha$, α , and 0° , respectively. The shapes of the focal arc and the lens contour can be determined by the following constraint equations. The parameters are indicated in Fig. 6.

- Electrical constraints:

$$F_1 \bar{P} \sqrt{\epsilon_r} + W + N \sin \beta = \sqrt{\epsilon_r} F + W_0 \quad (10a)$$

$$F_2 \bar{P} \sqrt{\epsilon_r} + W - N \sin \beta = \sqrt{\epsilon_r} F + W_0 \quad (10b)$$

$$\bar{G} P \sqrt{\epsilon_r} + W = \sqrt{\epsilon_r} G + W_0 \quad (10c)$$

- Geometrical constraints:

$$(F_1 \bar{P})^2 = F^2 + X^2 + Y^2 + 2FX \cos \alpha - 2FY \sin \alpha \quad (11a)$$

$$(F_2 \bar{P})^2 = F^2 + X^2 + Y^2 + 2FX \cos \alpha + 2FY \sin \alpha \quad (11b)$$

$$(\bar{G} P)^2 = (G + X)^2 + Y^2 \quad (11c)$$

Rotman lenses have found a wide range of applications in wireless communication systems. The size of a conventional

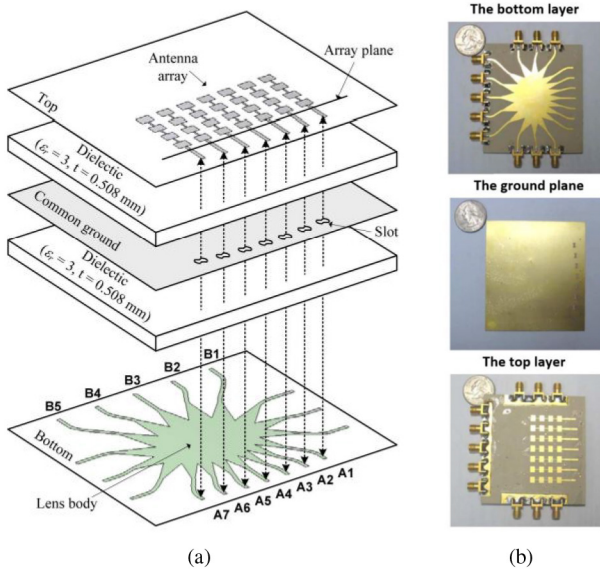


FIGURE 7. Two-layer Rotman lens-fed antenna array [30]. (a) Geometry consisting of a top metal layer, a dielectric substrate, a common ground plane, a dielectric substrate, and a bottom metal layer. (b) The fabricated prototype.

version is generally too large at lower operating frequencies compared to circuit type beamforming techniques. As a result, it is difficult to integrate them with base station antennas in cellular communication systems. After the invention of the Rotman lens it was proposed to reduce its size by loading the parallel plate region using dielectric material [27], [28]. Then the first microstrip Rotman lens with an expanded scan ability was introduced in 1967 [27]. Two-dimensional (2D) lens stacks for wide solid wide angle scans were introduced in 1970 [29].

The design of these lenses is typically performed with geometrical optics, but taking mutual coupling effects between the lens ports into account. The latter is relatively difficult to control, but the former is crucial to the realization of an efficient and compact lens. Thus, a careful geometrical optics design should be accomplished first; then adjustments must be made with full-wave simulations to reduce the mutual coupling effects.

Various methods and techniques have also been reported for reducing the sidelobe levels (SLLs) [31]–[37], increasing the scanning range [38], [39], realizing 2D scanning [40], improving the bandwidth performance [41]–[44], and miniaturizing the sizes of the Rotman lenses for applications in cellular systems [45].

A low temperature co-fired ceramic (LTCC) substrate Rotman lens was introduced in [46] that paved the way towards the realization of a completely integrated transceiver. The authors in [30] describe how to realize a compact Rotman lens-fed antenna array using a multi-layer configuration for 5G mmWave applications. The form of this lens-fed antenna consists of two layers. The design has a low profile and occupies a relatively small area. Consequently, it is attractive for applications where the form factor is important. The designed prototype is shown in Fig. 7.

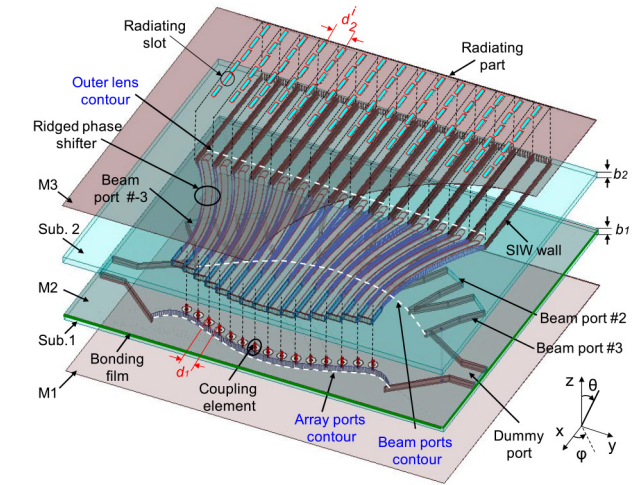


FIGURE 8. Dual-layer Rotman lens with ridged delay lines [48].

A dual-layer Rotman lens for applications in the 5G mmWave band was developed in [47]. The lens was implemented using a new transition based on several star-shaped coupling slots and an integrated reflector. Compared to the standard rectangular coupling slot transitions, it is broadband and maximizes the power transfer between the two layers of the lens regardless of the position of the beam port along the focal arc. This design was improved by the same research group using ridged delay lines to reduce its footprint [48]. It is shown in Fig. 8. The coupling elements along the array port contours were implemented with several cylindrical vias connected to ridged waveguide delay lines. The use of the cylindrical vias with azimuthal symmetry for the coupling transition and of delay lines in the ridged waveguides allowed an improvement in bandwidth for most of the scanned beams.

The use of substrate integrated waveguides (SIW) is a known successful technique for transmission lines at mmWave frequencies [49]. The original topology of the Rotman lens employed fixed coaxial cables with electrical lengths set by design, providing true time delay operation. To achieve a more compact configuration, an SIW phase shifting network, which is equivalent to the fixed-cable design over a moderate bandwidth, was introduced in [50]. This mmWave Rotman lens was realized with SIW technologies; it is shown in Fig. 9. A mmWave wideband high-gain multi-beam array antenna was developed in [51] using an SIW Rotman lens connected to parallel-fed slot antenna array. A dual-layer Huygens' unit cell based on offset electric dipole pair was also developed to serve as a superstrate of the multi-beam array to further enhance the gain. The maximum achieved gain was 24.4 dBi.

Rotman lenses provide a natural amplitude taper across the aperture which lowers the SLLs. However, for some applications with more stringent requirements, such as high beam-to-beam isolation, there is some interest in further reducing the SLLs. There are several common ways to reduce

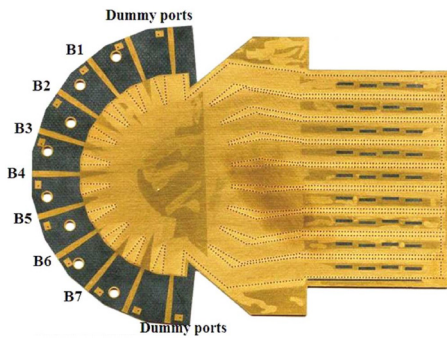


FIGURE 9. SIW-based Rotman lens [50].

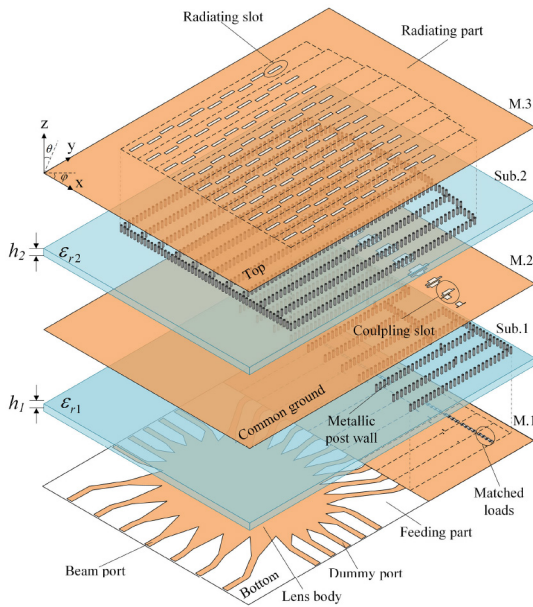


FIGURE 10. SIW-based dual-layer Rotman lens with reduced SLLs that delivers non-uniform amplitudes to the elements of a multi-beam slot array for SLL suppression [52].

the SLLs of multi-beam arrays fed by a Rotman lens. These include:

- Increasing the aperture size of each beam port to apply an edge taper to the array ports.
- Introducing a small lens as the prime feeding network to excite a large lens.
- Employing a dual port feeding method.
- Terminating the Rotman lens with lossy networks.
- Using active circuits, such as power amplifiers or phase shifters, to change the distribution of the amplitudes and/or phases.

A lossy network at the output of the Rotman lens was introduced in [52] to taper the amplitude distribution across it in order to reduce the SLLs. This design is shown in Fig. 10. Its amplitude distribution was controlled with a series of double-stepped SIW-based slot couplers that connected the Rotman lens to the radiating elements. These couplers regulated the coupling power; the design parameters were optimized to yield the phase values required to



FIGURE 11. Conformal SIW-based dual-layer Rotman lens [53].

attain the desired low SLLs. The double-stepped slot coupler was designed so that a part of the power from the array port in the lens layer would be coupled to the antenna layer to feed the slot array through double-stepped slots, while the remaining power was absorbed. Specifically, an SIW-based matching load was used to absorb the excess power in each SIW-based feed line in the lens layer. This solution achieved some antenna size reduction but at the expense of a relatively complex dielectric stack-up. Each feed line consisted of complex multi-layer dielectric stack-up of a transverse slot, four chip resistors, and a short-circuited wall.

A similar configuration was also developed to feed a cylindrically conformal slot array antenna in [53]. Photos of this prototype are shown in Fig. 11. Its conformal slot array consisted of 10×10 radiation slots. Its conformal Rotman lens was developed to be integrated with that conformal array and was mounted onto a cylindrical surface. The Rotman lens fed the slot array through the coupling slots in the broad sides of the SIW waveguides. Double-layer SIW phase shifters were introduced between the Rotman lens and the slot array to manipulate the phase distribution on the slots. While the phase shifter design in [53] is similar to that in [52], the chip resistors were not used. Consequently, the SLLs were no longer suppressed, but the overall efficiency of the multi-beam system was increased. Although the experimental validation in [52], [53] was performed at the lower frequency of 10 GHz, the concept is nevertheless relevant and fully applicable to mmWave frequencies.

A hybrid analog-digital beamforming system based on a Rotman lens was developed in [54]. A massive multiple-input-multiple-output (MIMO) system was achieved. Several Rotman lens designs have been reported for mmWave cellular systems in [55]–[57]. Rotman lenses realized with additive layer manufacturing (ALM) techniques were also reported in [58]. A ridged waveguide version was demonstrated to have superior performance when compared to conventional E-plane and H-plane lens designs [59].

C. LUNEBURG LENS

In all of the systems mentioned above, there are inherent system phase errors across the apertures for the majority of the multiple beams. They occur because constrained lens designs provide only a limited number of true focal points, resulting in a scanning range generally not exceeding $\pm 50^\circ$ [38]. From this point of view, Luneburg lenses [60]

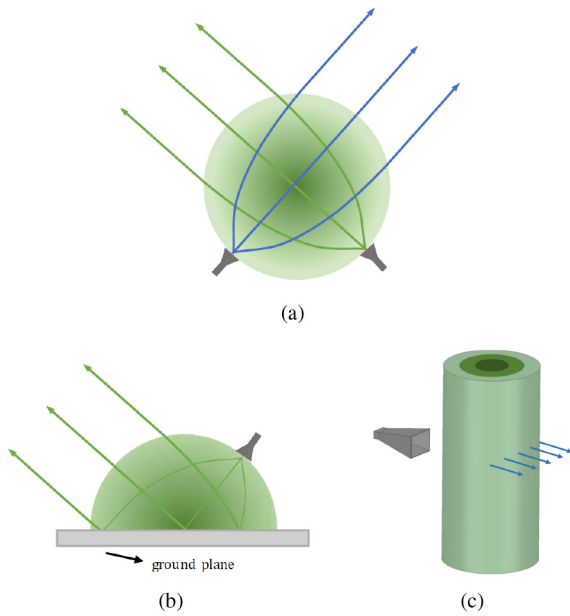


FIGURE 12. Luneburg lens shapes with the darker colour representing an increasing permittivity. (a) Spherical. (b) Half spherical. (c) Cylindrical [61].

and their derivatives would be the most desirable multi-beam lens antennas for achieving multiple beams, because they exhibit, in theory, no phase error for any pointing direction.

Spherical and cylindrical Luneburg lenses have a number of features that make them uniquely suitable for realizing multi-beam antennas with wide scanning range. Owing to their spherical or rotational symmetry, the beam shape, in principle, does not vary with the scan angle. To form a narrow beam in two dimensions, there is no need to employ a large number of radiating elements as the aperture forming the beam is the lens itself. No additional feed network is needed to radiate dual-polarization since the lens propagates orthogonal polarizations equally well provided the dielectric used to create it is reasonably isotropic. The original Luneburg lens is a dielectric sphere whose index of refraction follows the equation $n(r) = \sqrt{2 - r^2}$, where r is the normalized radius of the lens. Therefore, the lens naturally provides a refractive index that is 1.0 at its outer surface, thus making the reflection low for waves exiting it as they transition into the air. Because the lens design is based on an equal-path true time delay operation, it is inherently a wide-band structure. The dispersion of the dielectric employed is the only potential limitation. The beam may be steered as the feed moves around the surface as illustrated in Fig. 12.

The beamwidth produced by a Luneburg lens is primarily defined by its diameter and the corresponding projected aperture of the lens. If one places a number of feeds along the inner surface of a Luneburg lens, multiple beams can be produced on the other side, one beam per feed. The main advantages of Luneburg lenses over antenna arrays based on beamforming networks can be summarized as follows [62]:

- A great simplification in the component count and an inherent low passive intermodulation (PIM).
- Reduction of network losses.

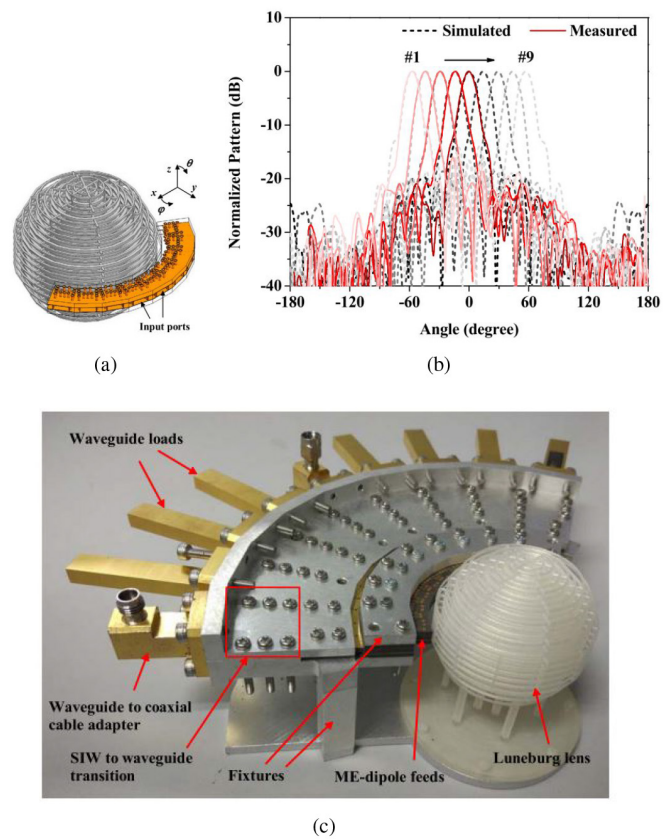


FIGURE 13. Luneburg lens based multi-beam antenna with multiple ME-dipole feeds. (a) Geometry. (b) Radiation patterns of the multi-beam antenna at 32 GHz. (c) Photo of the prototype of the multi-beam antenna developed in [10] with its connection adapters and waveguide loads.

- Beam crossover levels can be selected arbitrarily by properly choosing the spacing of the source elements.
- Isolation between elements is generally superior to that obtained with beam-forming networks.

On the other hand, the main disadvantage of Luneburg lens structures is their size and weight, which could be significantly problematic in practice. In this regard, reported works reveal various innovative implementations of Luneburg lenses [63]. Slim and cylindrical Luneburg lenses have paved the way for highly directive antennas with low profile structures [64]–[68]. Methods for the compression of the lenses are investigated in [69]. Different novel designs of parallel-plate Luneburg lens have been investigated that are capable of creating highly directive beams in their H-plane [70]–[74]. An appealing design of a cylindrical Luneburg lens with E-plane focused beams is presented in [75].

In general, a 2D scanning capability can be perfectly realized with an appropriately designed spherical Luneburg lens. Fabrication of the spherical layers with a varying dielectric profile remains a big challenge. It is very difficult and very costly to produce an ideal Luneburg lens, i.e., one with a continuous gradation of its dielectric constant. As a practical alternative, one can employ several separate shells to replace the theoretical gradation with a discrete approximation to

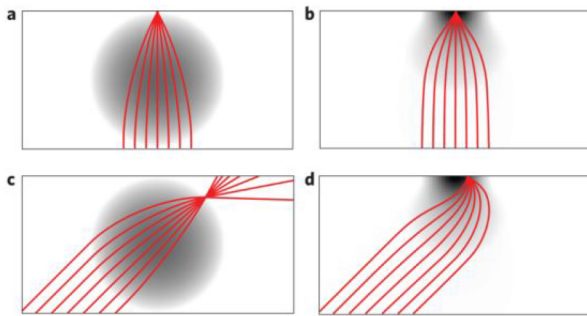


FIGURE 14. Ray tracing results for spherical, (a) and (c), and flattened, (b) and (d), Luneburg lenses. (a) Strong focusing of the rays. (b) Radiation patterns of the corresponding multi-beam antenna at 32 GHz. (c) Rays at oblique incidence are focused onto a spherical surface. (d) Rays at extreme angles are focused onto the image plane [85].

it [76], [77]. The focusing performance is then dependent on the number of shells approximating the theoretical graded-index [78]. Many such versions have been deployed in a variety of current systems. Various methods have been proposed for implementing the required graded-index profile. Sliced spherical Luneburg lenses with periodic holes drilled in the dielectric slabs have been reported in [79]–[81]. Another study considered a spherical lens using a polymer jetting rapid prototyping technique [82]. Unfortunately, alternative 3D methods such as polymer stereolithography are not suitable for low loss microwave communication systems. However, ceramic stereolithography was used in [83]. It resulted in low loss sub-wavelength structures with a high volume fraction of ceramics.

Recently, 3D printing techniques have demonstrated their potential for high accuracy fabrication at low cost. They have attracted serious attention from researchers on Luneburg lenses. A good example can be found in [10] where a novel 3D printed Luneburg lens fed by a dual-polarized magneto-electric (ME) dipole was reported. The design prototype created 9 beams over the entire Ka-band. It is a suitable candidate for multi-beam cellular applications. The structure is shown Fig. 13.

Luneburg lens antennas with a flattened shape [84] have been developed using transformation optics (TO) [13], [14]. Kundtz and Smith [85] used it to demonstrate a broadband broad-angle Luneburg lenses with a flat source-side surface. Ray tracing of the spherical and flattened Luneburg lenses are shown in Fig. 14. These illustrations demonstrate that with the TO-based index profile, even rays at extreme angles are focused.

Another 3D TO-based Luneburg lens with a flattened focal surface was introduced in [81]. The 3D lens is made of metamaterials with non-resonant inclusions. They were realized as multilayered dielectric plates drilled with inhomogeneous holes. The complete structure and the relations between the refractive index and the hole's diameter D are shown in Fig. 15 for different unit cells and different polarizations, P_1 , P_2 , and P_3 at 15 GHz. The prototype demonstrated high gain and narrow beams with wide scan angles.

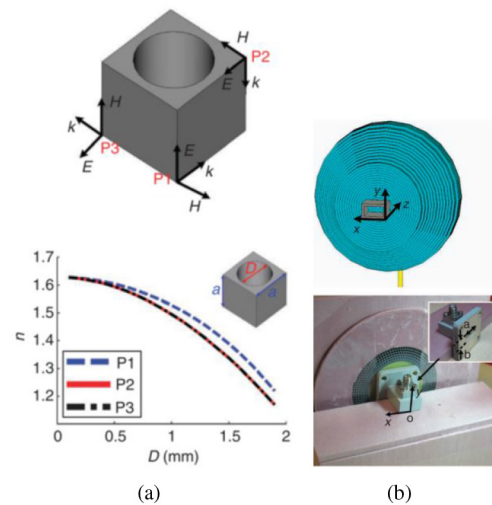


FIGURE 15. Components of the 3D transformation-optics (TO) based Luneburg lens [81]. (a) Relations between the refractive index and the hole's diameter D . (b) Photo of the source and it mounted on the lens.

A flattened Luneburg lens for the THz regime, based on the application of quasi-conformal TO, was reported in [86]. This design considered a reduction in the dimensionality of the lens, from three to two. A cylindrically symmetric design was developed in which the radiation is confined in the third dimension by metal plates (i.e., a parallel-plate waveguide). The fact that a parallel-plate metal waveguide, operated in the lowest-order transverse electric (TE_1) mode, acts as a 2D artificial dielectric was exploited. The effective permittivity that it can achieve at a given frequency was determined by the spacing between the two metal plates, similar to the engineering of the Ruze lens as described in Section II-A. This device offers a wide-angle beam steering capability and beam reception over a broad bandwidth. The design is scalable to any frequency band in the THz range.

Variations of the Luneburg lens have been investigated for mmWave applications. This includes the reflecting Luneburg lens [87], which is suitable for feeding leaky wave antennas upon reflection at the circumference of the lens; and the Gutman lens [88], which is characterized by a focus inside of the lens rather than on its surface. A recent design reported in [89] was realized with the fused filament additive manufacturing method. Another interesting lens design, providing the focusing properties of a planar Luneburg lens without any dielectrics, is the Rinehart-Luneburg lens. It is also known as the geodesic lens [90], [91]. The main drawback of this solution is its volume. Various other designs have been reported recently, including the folding of the lens profile to reduce its height while keeping its focusing properties [92]–[95]. These fully metallic designs are of interest for applications requiring highly efficient antennas.

III. METASURFACE-BASED TRANSMITARRAYS

To simplify the mechanical design of constrained lenses, McGrath proposed in [96] the use of planar surfaces both

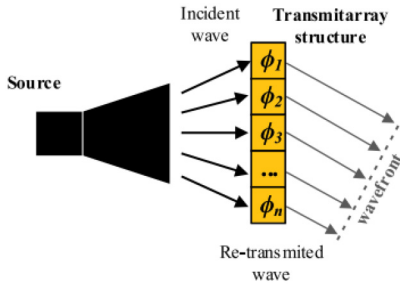


FIGURE 16. Illustration of a transmitarray [97].

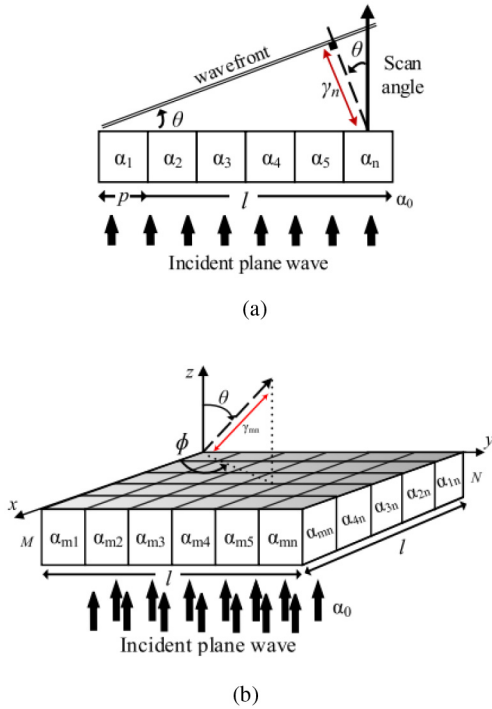


FIGURE 17. Illustration of the model of a transmitarray for (a) 1D beamsteering, and (b) 2D beamsteering [97].

in the front and the back of the lens, with a possible implementation consisting in simply connecting two microstrip patch array antennas on both sides of a ground plane using vias. This type of lens is typically a thin, multi-layered structure and is called a transmitarray; it can be planar or conformal [97]. Fig. 16 provides a schematic of the operating principle of a transmitarray. Transmitarrays based on printed circuit board (PCB) technology have received a lot of attention as they enable lightweight and inexpensive antenna solutions.

The principle of beamsteering using a transmitarray is that the phase shifting is obtained by controlling the phase delay introduced by each individual element of the transmitarray, as reported in [98]–[100]. In the same manner as a phased array, 1D beamsteering limits the applications of a linear transmitarray to steering in one azimuth/elevation plane. Similarly, 2D steering using a transmitarray is characterized by a planar array as shown in Fig. 17. The principle of operation

is the same as a phased array in that a progressive phase shift between adjacent elements should occur, for instance, along the x direction, or the x and y directions of the array to achieve 1D or 2D beam steering, respectively. In this regard, several transmitarrays for beam steering applications have been reported [101], [102]. Such designs benefit from having no feed blockage and the possibility of reducing the focal distance to obtain compact systems.

Novel methodologies have been reported in the literature to improve the bandwidth performance of transmitarray antennas through the control of the transmission phase range and by optimizing the phase distribution of the transmitarray elements [103]–[107]. Dual and multi-band designs have also been reported recently [108]–[110]. As the complexity and size of transmitarrays grow, more effective analyses and computation techniques will become necessary [111], [112].

A mmWave multi-beam transmitarray for Ka-band applications was reported in [113]. This design is optically transparent and offers the possibility of steering the beam in the horizontal plane from -30° to $+30^\circ$, both features facilitated by a novel meshed double-circle rings unit cell structure. This unit cell provides a phase shift of $+300^\circ$ for an insertion loss smaller than 1.0 dB at 28.5 GHz. The transmitarray design was successfully fabricated and tested. The antenna had a 9.9 wavelength diameter at 28.5 GHz. It produced a broadside gain of 25 dBi and a -1.0 dB gain bandwidth of 1.8 GHz. The simulated unit cell model and the final prototype are shown in Fig. 18.

Furthermore, transmitarrays are desirable for use and mounting on mobile platforms, such as aircraft, unmanned aerial vehicles (UAVs) and high-speed trains. Conformal designs are very desirable for such applications to meet their aerodynamic requirements. However, the design of transmitarrays exhibiting high performance characteristics whose structures are bent to conform to curved surfaces remains very challenging. First of all, most of the transmitarray designs to date have employed multiple thick frequency selective surface (FSS) layers to realize the required phase distributions, i.e., a 360° phase range with acceptable transmission loss [114]–[116]. A second problem comes with the need to conform to surfaces with a large curvature when the beam scanning capability is facilitated by the use of PIN and varactor diodes. Those elements and the requisite circuit layouts do not like to be bent.

Two novel high-efficiency, and ultra-thin conformal transmitarrays were introduced in [117], [118]. The ultra-thin conformal transmitarray consisted of three-layers of identical square ring slots. The associated FSS element and the final prototype are shown in Fig. 19. Each layer is separated by a distance of only 0.02λ at 25 GHz. Therefore, the entire thickness of the element is about 0.04λ (0.508 mm), making it suitable for bending. The element is fed by a standard horn with about a 10 dBi gain. Then, the feed source is rotated at the feed point to allow steering the beam to the angles: 0° , $\pm 5^\circ$, $\pm 10^\circ$, and $\pm 15^\circ$. It was fabricated and tested successfully. The authors have since

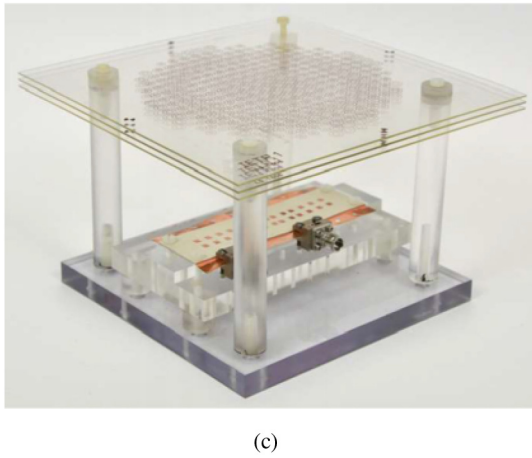
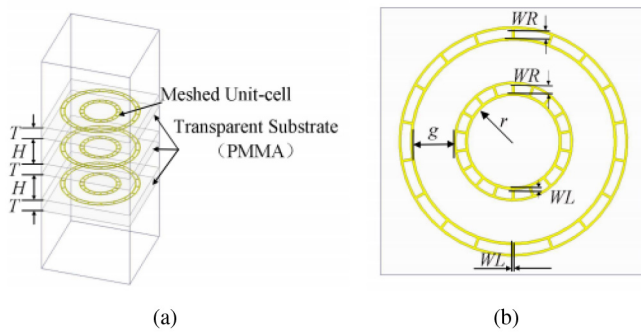


FIGURE 18. Conformal transmitarray reported [113]. (a) Perspective, and (b) Top views of the meshed double-circle rings unit cell used to realize it. (c) Photographs of the assembled prototype.

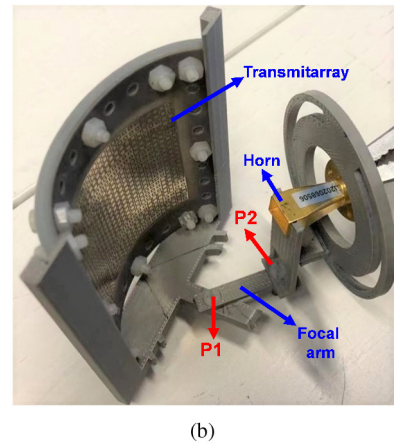
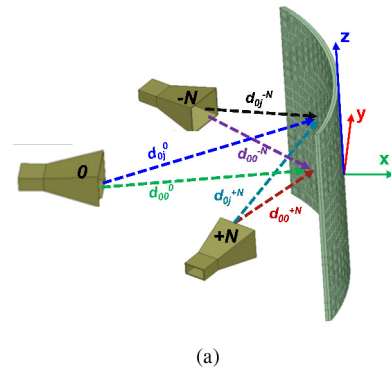


FIGURE 20. Conformal transmitarray prototype reported in [16]. (a) 3D schematic of the transmitarray configuration and its horn feed in multiple feed positions. (b) Photograph of the fabricated prototype (perspective view from one side).

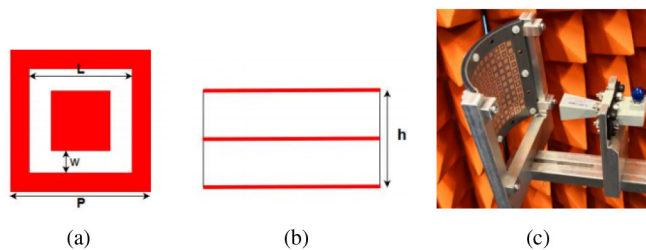


FIGURE 19. Conformal transmitarray prototype reported in [118]. (a) Top, and (b) Side views of the FFS element used to realize it. (c) Photograph of the assembled prototype as the antenna-under-test.

modified the structure using the same FFS element. They report a mmWave wide-angle multi-beam conformal transmitarray [16]. Its prototype is shown in Fig. 20. The multi-beam radiation angles cover a range of $\pm 43^\circ$ with a 2.7 dB scan loss.

Reconfigurability is another feature that can be applied to transmitarray designs [119], [120]. To make a transmitarray reconfigurable, one needs to control the phase shift produced by each unit cell. The main beam direction and its shape can then be changed dynamically. This phase shifting functionality can be implemented with different technologies. They include different materials, unit cells designs, and implementation approaches.

In regards to B5G and 6G applications, very few transmitarrays have been demonstrated beyond 100 GHz with PCB technologies. Lack of progress at those higher frequencies is mainly due to fabrication constraints. Nevertheless, a three-layer high-gain D-band transmitarray fabricated with standard PCB technology was presented in [121]. Three flat lenses comprised of 1600 elements were designed to generate broadside and scanned beams. The lens design was based on a 3-bit quantization of the 360° phase range. This choice reduced the directivity loss by ≈ 0.3 dB, as well as the number of cells (eight) to be simultaneously optimized over the targeted band. The consequent 40×40 broadside transmitarray based on those optimized cells outperforms the transmitarrays presented so far in the 100–300 GHz band in terms of its -1.0 dB gain bandwidth, 11.7%. Two scanned-beam transmitarrays with on-axis feeds were also characterized to experimentally assess the scan loss and the performance of the cells under oblique incidence. A linearly polarized pyramidal horn was employed to measure the radiation patterns. The unit cell designs and the transmitarray architecture are shown in Fig. 21.

At higher frequencies such as those in the THz region, graphene substrates have attracted researchers' attention for

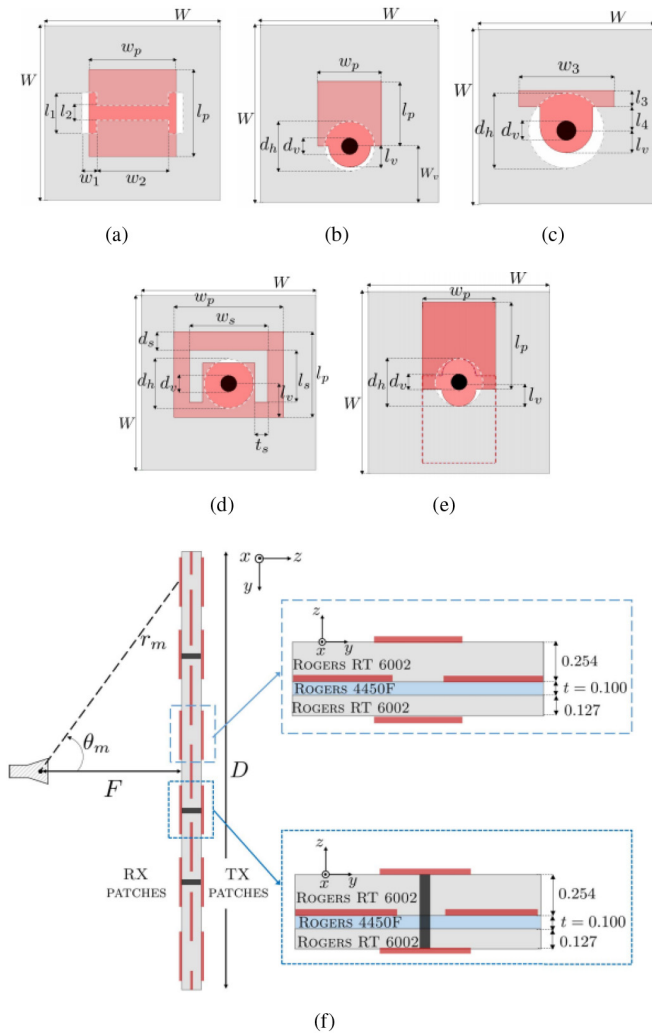


FIGURE 21. Transmittarray design reported in [121]. Unit cell (UC) designs: (a) UC1, UC2, and UC3 (aperture-coupled patches); and (b) UC4, (c) UC5, (d) UC6, (e) UC7, and UC8. (Red solid and red dashed lines: outer patches. The ground plane is depicted in gray, the vias in black.) (f) Architecture and stack-ups of the two types of unit cells employed, i.e., the aperture-coupled and via-connected patches. All dimensions are in mm.

transmittarray designs because they can support surface plasmons with high confinement and low losses. Moreover, their carrier density can be tuned with an external gating voltage. Thus, one can attain tunability of its plasmonic responses [122]–[124]. PCB technology is a competitive approach and has been employed for the realization of a low cost two-layer THz transmittarray design [125]. The design employs a novel element which has a simple structure that consists of two metallic layers on different sides of a substrate. As was demonstrated, it has a maximum transmission loss of 3.52 dB and a full 360° phase coverage at 250 GHz. A transmittarray was designed based on this element that had a low focal-to-diameter ratio (F/D) of 0.3 at 250 GHz. A standard WR-03 open-ended waveguide with a wall thickness of 12.5 mm was used to feed the transmittarray to decrease the backward radiation. The unit cell design and the final prototype are shown in Fig. 22.

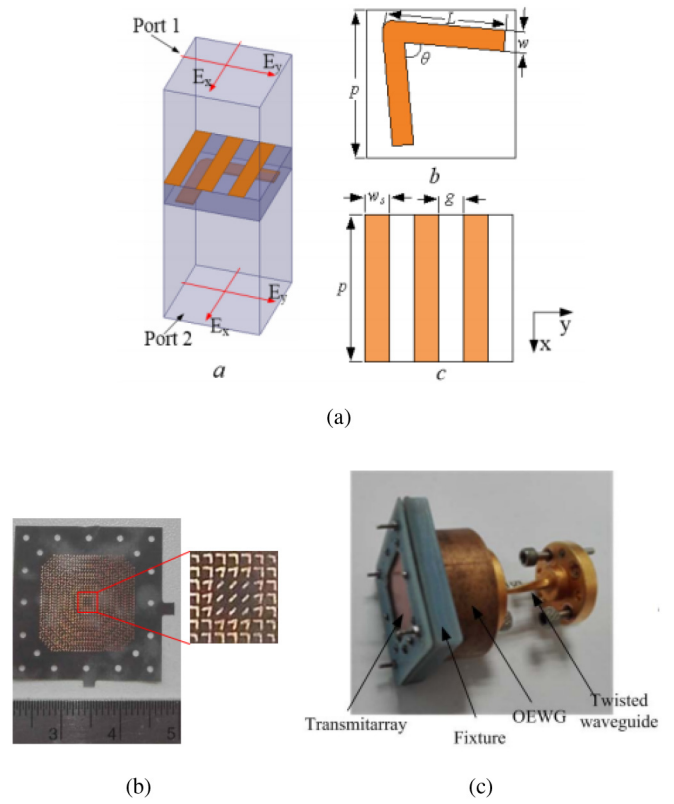


FIGURE 22. Fabricated and measured 250 GHz transmittarray reported in [125]. (a) Simulation model of its two-layer unit cell consisting of the depicted V-shaped element printed on the bottom of the bottom layer and the metallic grating printed on the top of the top layer. (b) Photograph of the front of the assembled transmittarray. (c) Fabricated prototype with its feed and fixture structures.

IV. REFLECTOR BASED MULTI-BEAM ANTENNAS

Reflectors, like lenses, are among the aperture antennas developed with geometrical optics. Much like mirrors in the optical domain, they utilize one or more shaped reflective surfaces that are illuminated in a prescribed manner to achieve their desired radiation characteristics.

The types of reflectors employed in the realization of multiple beams can be divided into two simple categories: single reflectors and dual reflectors. A single reflector example is the cylindrical parabolic-shaped structure that was combined with the constrained lens reported in the original paper by Rotman and Turner [24]. When its feed is positioned at the focal point F of the parabola, the cylindrical waves that are produced upon reflection combine into a plane wave traveling in the direction perpendicular to the parabola’s aperture. Doubly curved reflectors can also produce a similar plane-wave characteristic with fan beam shapes [126], [127] or pencil beams when fed by a line source [128].

Dual-reflectors realized with Gregorian and Cassegrain geometries can be used to produce similar focusing properties, generally with a more compact implementation [129]. The plane waves generated from the reflectors can then be used to excite an antenna array. When a single source is placed at the focal point, a single beam output is attained.

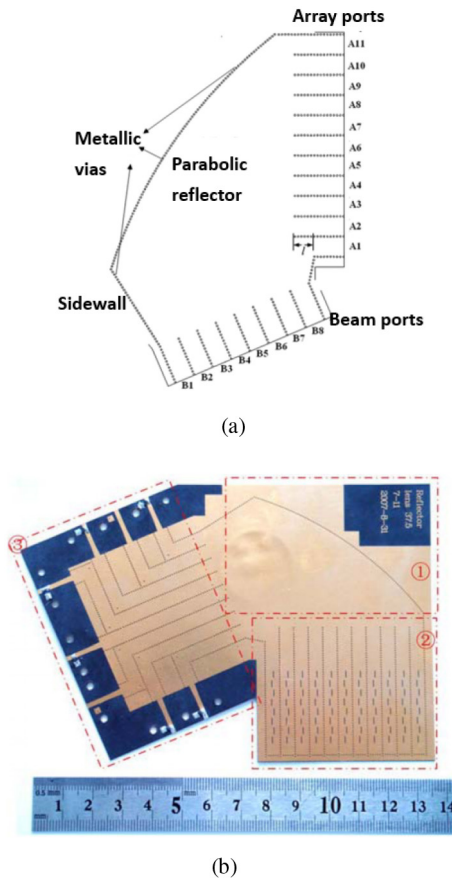


FIGURE 23. SIW-based offset-fed parabolic reflector reported in [130] based on the parabolic reflector principle. (a) System configuration which consists of an SIW-based parabolic reflector, an SIW slot array antenna, and its feed lines. (b) Photograph of the fabricated SIW multi-beam antenna.

A multi-beam array requires multiple excitations placed at other positions away from that focal point. When the excitation is not at the focal point, the wave front and phase relationships change and a tilted beam is realized. Details of both dual-reflector systems are described below.

A. SINGLE REFLECTORS

Two types of single reflectors, i.e., offset-fed and pillbox antennas [131] with single-layer and double-layer parallel plate waveguide configurations, respectively, are typically employed as beamformers. The determination of the scattering characteristics of a single parabolic shaped reflector begins with its geometrical definition, i.e., its shape defined relative to an x - y coordinate system:

$$y^2 = 4Fx, \quad (12)$$

where F is its focal length. Both aperture blockage caused by its physical support structures and its feed can be eliminated with an offset-fed parabolic reflector design. A planar parabolic reflector was realized in [130] following this concept and using SIW technology. It is illustrated in Fig. 23. The feed network consists of a cylindrical parabolic reflector realized with a series of metallic vias and multiple open

SIWs which generate the cylindrical wave. An SIW slot array was designed and connected to this feed structure. Such a cylindrical reflector, which is sandwiched between two metal plates, can be easily integrated with SIW-based circuits and radiators. It is known as a pillbox reflector.

Another interesting example is the high impedance surface (HIS) reported in [132] that is fed by multiple offset pillbox reflectors. It is illustrated in Fig. 24. The feed structure is similar to that in [130], but four of them are employed to illuminate the square HIS from each of its four sides. By launching a surface wave towards the HIS from these different directions, each reflector covers one quarter of the intended angular range. The HIS is realized with microstrip patches and serves as the main radiator. This unique low profile configuration facilitates the realization of a multi-beam antenna that produces a full conical scan.

Unfortunately, the offset-fed configuration causes unbalanced phase and amplitude distributions that lead to undesirable features in the patterns of the output beams. To overcome this asymmetry problem, the pillbox configuration shown in Fig. 25 was developed in [133]. It integrates a 2D parabolic reflector realized with metallic pins and metal side walls into a dual-layer structure that yields symmetric patterns radiated by an SIW-based slot array. The feeding and radiating parts of this dual-layer configuration are hosted by two dielectric substrates. The bottom layer is a pillbox reflector with a mechanically rotating feed. The top layer consists of 23 waveguides, each having eight radiating slots. The coupling between the pillbox reflector and the radiating layer is realized using coupling slots etched in the conductor between them. The energy in the cylindrical wave produced in the bottom layer of this configuration is totally transmitted through the coupling slots into the upper layer, i.e., the coupling layer ideally causes no reflections. This type of symmetric structure can be used to obtain more balanced phase and amplitude distributions on the radiation portion of the system. Several multi-beam arrays have been realized as an extension of this pillbox configuration [134]–[138].

The sidelobe and beam crossover levels are interdependent in a multi-beam antenna system based upon a single radiating aperture. Low SLLs lead to low beam crossover levels, and vice versa [139]. For many applications such as cellular networks, however, this feature is undesirable. It was proposed in [140] to overcome this limitation using the so-called “split aperture decoupling method” which employs two radiating apertures. Each aperture is associated with a quasi-optical pillbox system integrated with several feed horns in its focal plane. Interleaving beams generated by the two separated beamformers provides the flexibility in controlling the SLLs and the beam crossover levels independently. The simulation model is shown in Fig. 26.

The modified pillbox reflector multi-beam array developed in [141] is shown in Fig. 27. Two extra parabolic reflectors were introduced into the quasi-optical system to reduce the SLLs. They were placed on both sides of the central parabolic reflector. Moreover, metal posts were added into

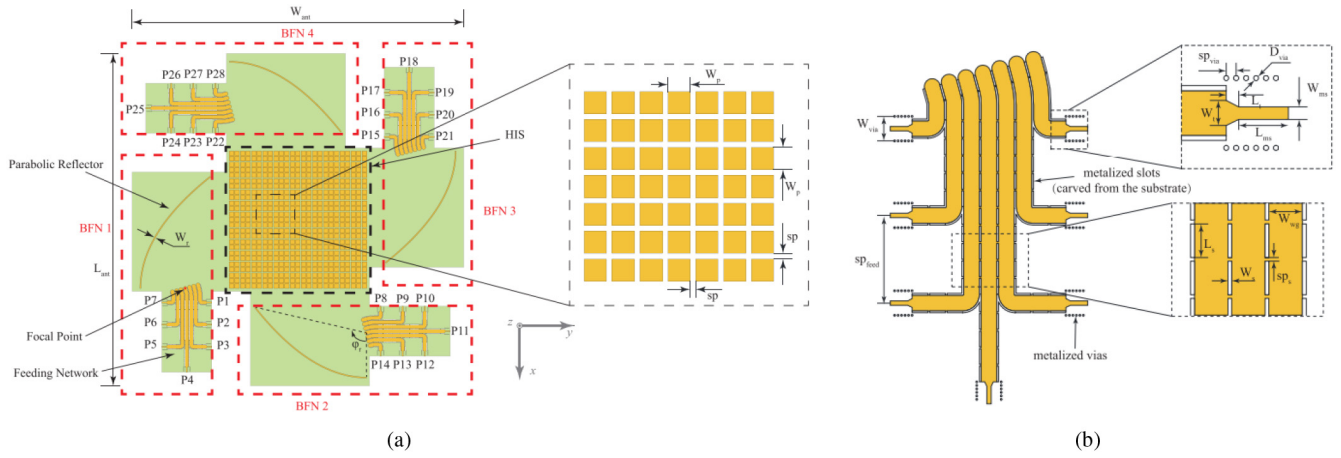


FIGURE 24. SIW-based offset-fed parabolic reflector lens that realizes full azimuth coverage [132]. (a) Overall configuration of the reported antenna. (b) Configuration of its feed network.

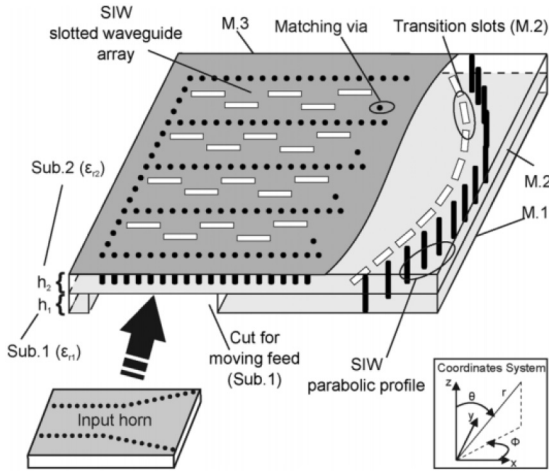


FIGURE 25. SIW-based pillbox-configured multi-beam slot array. There are three metal layers denoted as M_i , with $i = 1, 2, 3$. M_1 is the bottom wall of the pillbox reflector. M_2 is the top wall of the pillbox as well as the host of the coupling slots. M_3 is the layer that hosts the radiating slots [133].

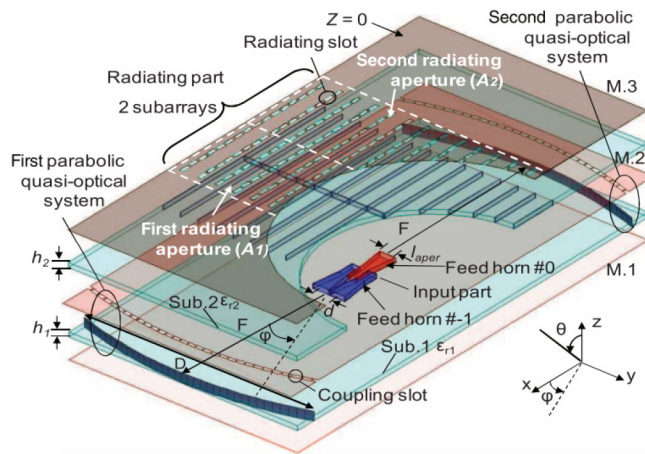


FIGURE 26. SIW-based pillbox-configured multi-beam slot array realized with the split aperture decoupling method [140].

the antenna array section to achieve a further reduction in the SLLs. The additional metal posts helped cancel the reflections arising from the slot array.

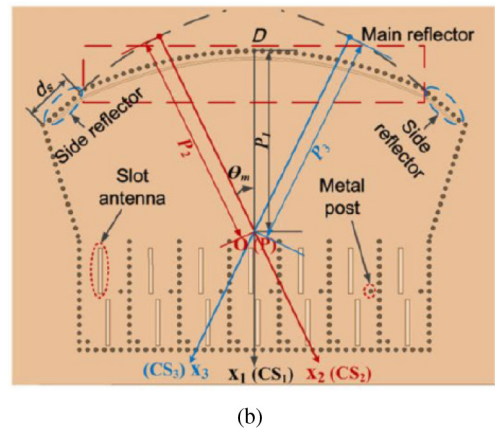
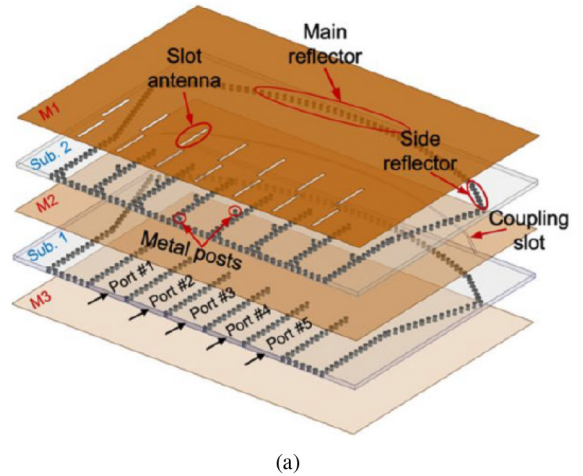


FIGURE 27. SIW-based modified pillbox reflector-fed multi-beam slot array with reduced SLLs [141]. (a) Perspective view. (b) Top view.

B. DUAL REFLECTORS

The single reflector examples presented above included offset-fed and pillbox configurations. Both can be extended to dual-reflector systems. Two examples of dual-reflector systems employing different configurations are shown in

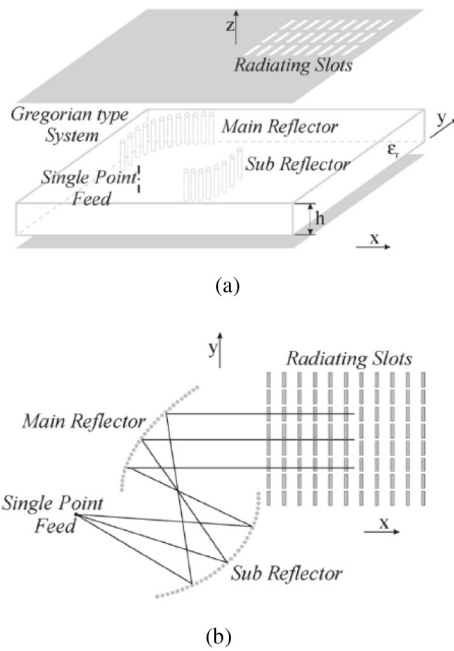


FIGURE 28. Multi-beam slot array fed by a dual offset Gregorian reflector system [142]. (a) Perspective view. (b) Top view.

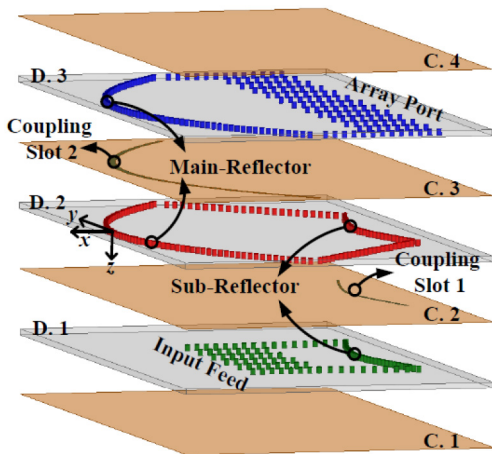


FIGURE 29. SIW-based Cassegrain lens BFN for a multi-beam array [143]. (The symbols “D.” and “C.” represent a dielectric and a conductor, respectively).

Fig. 28 and Fig. 29. The first one is a dual offset Gregorian reflector system that is used to feed a leaky-wave antenna [142]. The perspective and top views of this design are shown in Fig. 28. Since the design is a simple 2D version of the classic 3D Gregorian configuration, more details can be found in [129], [143]. Note that only one point feed was included and, hence, only one beam was generated in [142]. The beam-steering properties of this multi-beam array were realized by using leaky-wave antennas.

The second example shows the topology of a folded Cassegrain lens similar to the one reported in [135]. The electromagnetic wave transmission between adjacent layers was realized by introducing a coupling slot in the common conductor layers, C. 2 and C. 3. As shown in Fig. 29, the

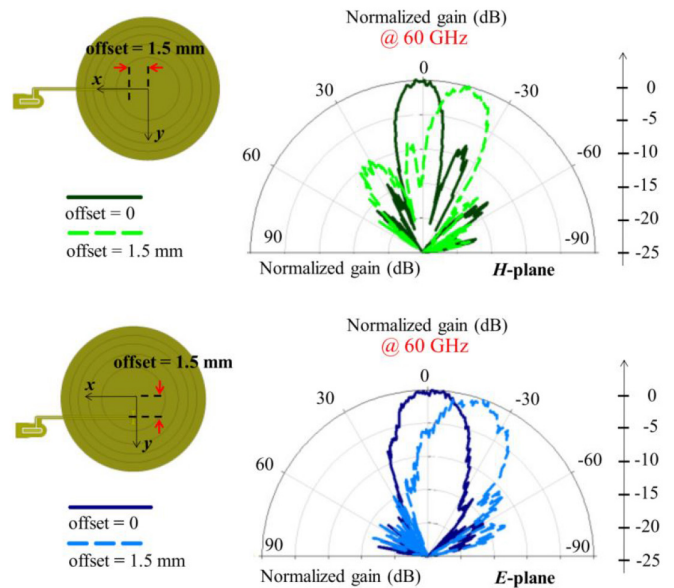


FIGURE 30. Comparison of the measured radiation patterns in both the E- and H-planes of the fabricated antenna reported in [145] that had a zero-feed offset with the one that had 1.5 mm offset.

coupling slot 1 is etched into C. 2. It is responsible for the transmission of the fields between D. 1 and D. 2. Similarly, the coupling slot 2 in C. 3 is responsible for the transmission between D. 2 and D. 3.

Multiple beam reflector antennas with a simple single feed per beam are often used for satellite ground station applications. A high-gain multi-beam bifocal dual-reflector antenna was presented in [144] for those applications. The antenna had a nearly square aperture with a 191λ side length at 12.75 GHz. Consequently, it realized a high gain and a wide scanning range. Moreover, it provided a wide field of view. Hosseini *et al.* presented a V-band high-gain quasi-parabolic reflector in [145] with a feed that radiates toward the reflector aperture. The reflector surface is formed by using concentric metallic/printed strip rings printed on different layers. Two possible excitation methods were proposed to provide beam-steering capabilities. The structure is shown in Fig. 30.

C. REFLECTARRAYS

Reflectarray antennas were first introduced in the 1960s to combine some of the advantages of both array theory and geometrical optics. They provide a flexibility to array designs because they have no need for complex beamforming systems [146], [147]. A reflectarray consists of a surface or aperture that is characterized by a surface impedance, and a primary radiator that illuminates it. The amplitude and phase of the fields reflected from the surface are determined by the impedance presented to an incident wave at every point on it. A low-loss reflectarray design provides control primarily over the phase of the reflected wave. This operating principle is schematically illustrated in Fig. 31. Prescribed radiation characteristics are then achieved by synthesizing the requisite surface impedance in a straightforward manner.

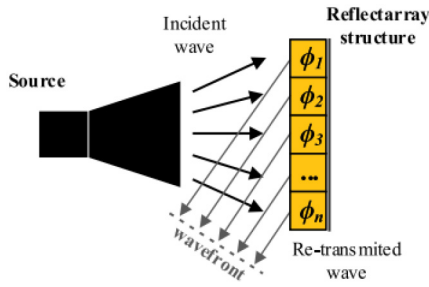


FIGURE 31. Illustration of a reflectarray antenna [97].

Reflectarrays bring advantages such as higher aperture efficiency, low SLLs and relatively high operating frequency bandwidths along with low fabrication costs [148]. These features makes them suitable for many applications such as satellite communications, radars, remote sensing, and radio astronomy.

V. TERAHERTZ LENS ANTENNAS

Data rates in 6G are promised to be even higher than those of 5G [149]–[151]. Much wider spectra are needed to accommodate such 6G expectations. Unfortunately, a large currently unoccupied spectrum does not exist below 100 GHz. Consequently, it is envisioned that 6G will largely occupy a significant portion of the THz range of frequencies [150]. Along with terrestrial-based communication systems, it is anticipated that THz systems will also play a role in space-based communications [152].

Currently, the most common definition of the THz band is that it encompasses of all of the frequencies from 0.3 to 3.0 THz. However, this definition has been loosened to include frequencies down to 100 GHz, so some sub-mmWave antennas are also called THz antennas. Recall that the wavelength in free space at 0.3 THz (300 GHz) is just 1.0 mm. Owing to the fact that THz wavelengths are then even smaller than mmWave ones, very narrow multiple THz beams with low probability of intercept (LPI) could be generated from physically very small areas. Moreover, beam steering and target tracking will remain indispensable features for the corresponding THz transmitting and receiving systems.

Signal attenuation in the lower portion of the THz range is even more severe than in the mmWave band. As a consequence, high gain antennas are even more necessary for anticipated 6G operations. Other important THz technologies that must also be developed to address 6G expectations are high power sources and highly sensitive receivers [153].

Exciting a large array of THz antenna elements, each 0.5λ in size, using a corporate feed network is a daunting engineering task. Therefore, it has not been favoured to date. Instead, a more promising approach has been to employ an electrically large lens fed by a simple element such as a dipole antenna or a small antenna array. To ease the associated problem of the need to precisely align the antenna with the lens, one could integrate the feed antenna with the lens.

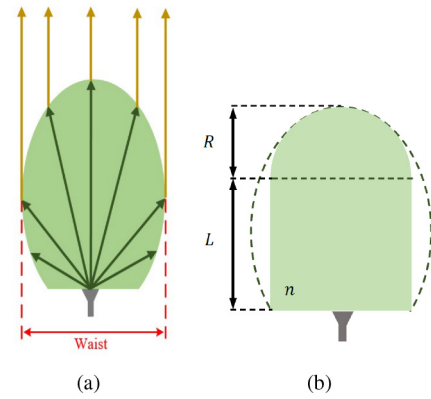


FIGURE 32. Illustration of integrated lens antennas. (a) Elliptical version. (b) An extended hemispherical lens antenna.

Antennas with this characteristic are known as integrated lens antennas [153]–[155].

A number of different types of lens antennas operating in the mmWave and THz bands have been reported [154]–[158]. These include the elliptical, extended hemispherical, and Fresnel zone lens. Each has its own unique physical and performance characteristics.

A homogeneous elliptical lens has two focal points. It can transform the radiation pattern arising from the feed being placed at one focal point into a plane wave exterior to the lens and propagating in the direction of the second focal point. Assuming that a represents the major semi-axis, b represents the minor semi-axis, L_{focal} represents the distance from the focal point to the centre of the ellipsoid, and n is the index of refraction of the dielectric from which the lens is fabricated, one has the following relationships:

$$a = \frac{b}{\sqrt{\left(1 - \frac{1}{n^2}\right)}} \quad (13a)$$

$$L_{focal} = \frac{a}{n} \quad (13b)$$

An integrated elliptical lens antenna is obtained by cutting off the part of the dielectric below the bottom focal point and placing the feed antenna beneath it. As depicted in Fig. 32, only the rays that hit the surface of the elliptical lens above the plane of its maximum diameter, denoted herein as its waist, are collimated. The portion of the radiated fields intersecting the lens below its waist are not collimated, but rather propagate along undesired directions or excite surface wave modes. These unwanted fields thus give rise to side lobes and other perturbations in the lens' radiation pattern [153]. One solution to this problem is to control the beamwidth of the feed antenna in order that the majority of its radiated energy falls within the angular range above the waist of the lens.

An optimized lens antenna operating at low THz frequencies and based on a tapered extension was developed in [159]. It had improved SLLs and gain performance in

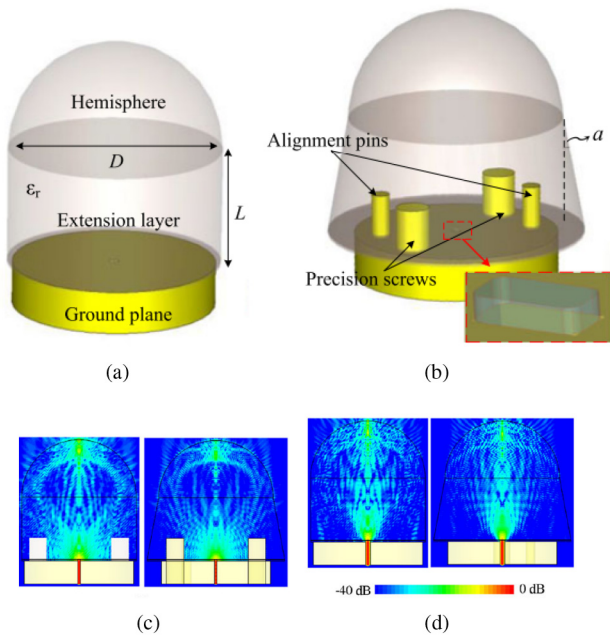


FIGURE 33. Basic geometry of an extended hemispherical dielectric lens antenna, where ϵ_r is the dielectric constant, D is the lens diameter, and L is the length of the extension layer [159]. (a) Antenna geometry that facilitates incorporating a WR-3 flange. (b) A narrowing of the extension is performed with respect to the tapering angle α . The inset shows the corresponding waveguide aperture with an air pocket present over it, the air region being colored blue for better visualization. Magnitude of the electric field inside the lens with and without tapering. (c) E-plane. (d) H-plane.

comparison to standard designs. A novel matching technique based on an air pocket etched out of the dielectric was employed to obtain broadband operation. This design is shown in Fig. 33.

Another issue arising from the internal reflections at the surface of an elliptical lens is the matching of the feed. One inherent characteristic of elliptical lenses is that all of the reflected rays that pass through the second focal point are reflected back to the first focal point. This reflected power causes a substantial mismatch to the feed impedance. A classical method to address this issue is to enclose the elliptical length with a matching shell that is a quarter-wavelength thick. The shell dimensions are specified according to the following equations:

$$n_{match} = \sqrt{n_1 n_2} \quad (14a)$$

$$h = \frac{\lambda}{4n_{match}} \quad (14b)$$

where n_1 , n_2 and n_{match} represent the refraction indexes of the lens; the air and the matching shell; and h is its height. The main drawback of this approach is that the improved matching performance can only be maintained within a relatively narrow bandwidth.

To improve the bandwidth one can incorporate multiple consecutive matching layers to perform a gradual transition between the two dielectric constants across each interface. Since the collimation of the rays from an elliptical lens only occurs for the portion of the wave front that impinges on its front surface, the part below its waist can be replaced

with a cylinder having the same permittivity. Furthermore, the top elliptical part, a hemi-ellipse, can be approximated by a hemisphere. This modification significantly reduces the fabrication complexity.

The difference in the height of the hemi-ellipse and the hemisphere can be compensated by the height of the cylindrical extension. This new lens is known as an extended hemispherical lens. It turns out to be a rather good approximation to a true elliptical lens although it tends to produce a slightly lower directivity in comparison to one having the same diameter. The relationship between the radius of the hemisphere, R ; the length (height) of the cylinder under it, L_{hemi} ; and the refraction index of the lens material, n , is given by:

$$L_{hemi} = \frac{R}{n-1} \quad (15)$$

A hyper hemispherical lens is similar to the extended hemispherical lens. In contrast to (15) the cylindrical extension length is now given by [155]:

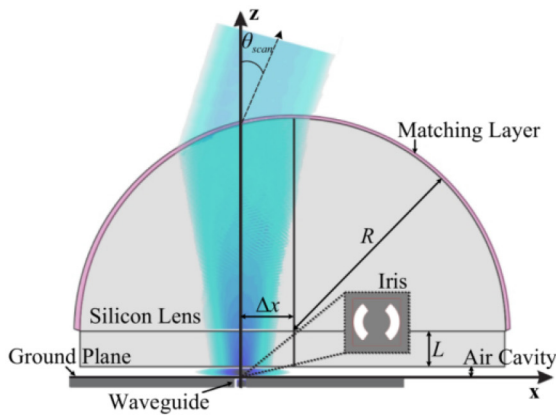
$$L_{hyper} = \frac{R}{n} \quad (16)$$

The rays at the output of a hyper hemispherical lens are not collimated. Therefore, the beam that it generates is much broader than that of the extended hemispherical lens. Nevertheless, it does sharpen the beam radiated by the feed antenna and increases its gain by a factor of n^2 . However, unlike the collimating lenses, the directivity of this lens does not increase with the lens size, i.e., its aperture size. The hyper hemispherical lens length satisfies the Abbe sine condition so it is free from coma aberration when the feed is transversely displaced from the lens axis [158]. Therefore, it is well suited for beam steering.

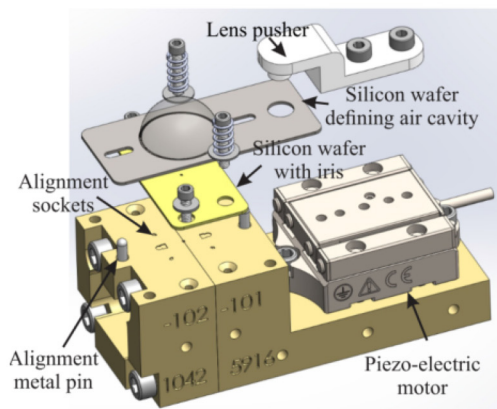
Beam scanning of a silicon lens antennas using integrated piezomotors at THz bands was reported in [160]. It demonstrated the integration of piezoelectric technology in receivers in order to enable a low power, mass, and volume beam scanning mechanism. This lens antenna could enable future space instruments as a replacement for the current bulky optomechanical systems thanks to the piezoelectric motors integrated with it, which are lightweight and low power. This design is shown in Fig. 34.

It must be noted that equations (15)-(16) are based simply on geometrical optics and point source assumptions. For actual antenna designs at mmWave and THz frequencies, optimization of the cylindrical extension with numerical simulations would be required to achieve the optimal radiation performance [161].

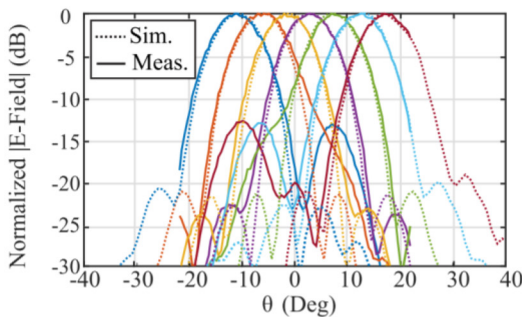
Designs of electronically steerable mmWave integrated lens antennas have been reported in [162]–[164]. The antennas in those designs are basically extended hemispherical quartz lenses fed with aperture coupled microstrip [162] and horn [163] antennas. The antennas provide electronic steering of the main radiation pattern beam by switching between antenna elements placed on the plane focal surface of the lens.



(a)



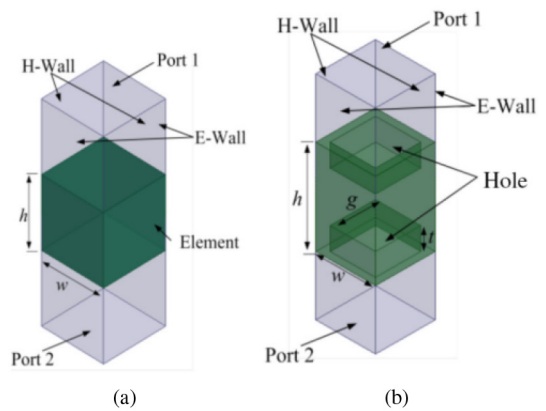
(b)



(c)

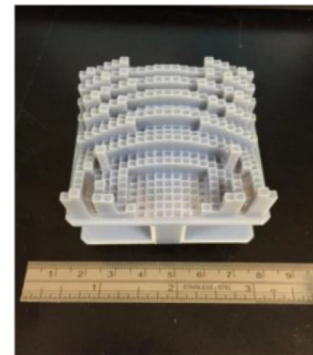
FIGURE 34. Scanning silicon lens antenna. (a) Geometry. The lens, $R = 6.0$ mm, is fed with leaky-wave waveguide. It is translated vertically from the waveguide nominal position to produce the scanning of the beam. (b) Drawing of the assembly of its prototype at 550 GHz with an integrated piezoelectric motor. (c) Measured (solid line) and simulated (dashed line) radiation patterns at 550 GHz for different lens positions [160].

Recently, 3D printing technology has facilitated the low cost fabrication of mmWave and THz dielectric lenses [165], [166]. Both 3D printed mmWave and THz lenses with fixed and scanning beams were studied in [167]. Periodic antireflection (AR) structures were added to reduce the impedance mismatch at the air-dielectric interfaces and led to higher directivities. To realize a beam-scanning lens a



(a)

(b)



(c)

FIGURE 35. Schematic model of lens phasing elements. (a) Without AR structure and boundary condition. (b) With AR structure. (c) Photograph of the prototype frequency-scanning lens realized with the AR structure [167].

dielectric post was introduced for phase control of the lens elements. Phase tuning was achieved by varying the height of the dielectric post in each unit cell. The schematic model of lens phasing elements without the AR structure and with it are both shown in Fig. 35.

A low cost 3D printed wideband mmWave extended hemispherical lens integrated with a dielectric circular polarizer was described in [168]. A novel high-gain circularly polarized discrete dielectric lens antenna operating at 300 GHz was realized with 3D printing in [169]. This circularly polarized lens was fed by a commercially available standard linearly polarized pyramidal horn. The lens works as a linear-to-circular polarization converter and provides the requisite transmission phase shifts to compensate for the spatial phase delays from the phase center of the feed horn to different pixels.

Another type of lens for mmWave and THz operations is the Fresnel lens [170]. A Fresnel lens consists of a number of alternately transparent and opaque half-wave zones. The source of the antenna is placed at its focal point. The opaque zones are attained by covering the corresponding portions of the lens with conducting or absorbing materials. Fig. 36(a) shows a circular Fresnel lens. It consists of a series of zonal openings in a finite conducting sheet. To increase the antenna efficiency and reduce the SLLs,

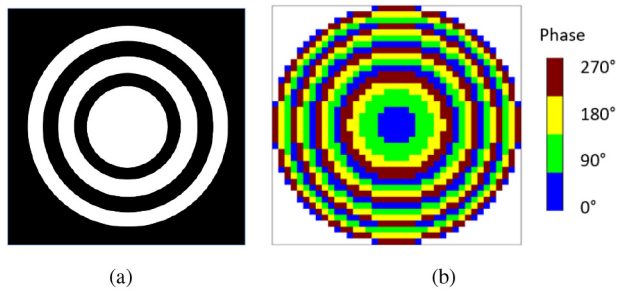


FIGURE 36. Illustration of Fresnel lenses. (a) Original Fresnel lens. (b) Circular phase correcting version [171].

one can introduce phase correcting elements into the zones as depicted in Fig. 36(b) [171]. The resulting radiator is effectively a transmitarray.

One salient advantage of the Fresnel lens is its low profile. On the other hand, its main disadvantages are its relatively narrow bandwidth and low efficiency. If one replaces the opaque and transparent regions with phase correcting elements, one would obtain a true transmitarray. Substantial progress has been made to increase the bandwidth of transmitarrays in recent years [172]. It should be pointed out that although a Fresnel lens can be made flat, it still needs a feed antenna typically placed many wavelengths away from the lens. If the required beamwidth is not too narrow, one can achieve a completely flat version, i.e., a metasurface-based antenna, by placing a metasurface above an antenna backed by a ground plane [173].

VI. FUTURE RESEARCH CHALLENGES

Future mmWave and THz communications systems demand multi-beam antennas. The multiple beams they radiate are required to be individually and dynamically steerable. Quasi-optical configurations serve as very promising solutions. However, to make such systems work in practice, a number of challenges remain to be addressed. The first one is to develop cost effective ways to fabricate the lenses and reflectors with high precision and low loss. Although 3D printing has served as a promising technology, the machines and materials for printing high performance mmWave and THz lens and reflector antennas are not yet mature enough. The second one is the need to design and realize smart feeds that have dynamic beamforming abilities and that can be readily integrated with the lenses and reflectors. The third one is the need to achieve accurate and cost effective beam tracking capabilities. One can realize very high gain and narrow beams at mmWave and THz frequencies with a physically moderate or even a small aperture. However, for all practical applications in a dynamic or mobile environment, these narrow beams need to be tracked with a high accuracy in order to maintain a resilient radio link. To achieve this without resorting to auxiliary sub-systems, such as the global positioning system (GPS), remains a challenging task. Combining lens and reflectors with digital beamforming to form hybrid arrays is potentially a viable solution [1].

VII. CONCLUSION

This paper presented an overview of quasi-optical mmWave and THz multi-beam antennas for B5G and 6G terrestrial and non-terrestrial network applications. Various conventional lenses and advanced lenses such as transmitarrays and planar lenses based on transformation optics were discussed. Single and double reflector configurations suited for mmWave operation were described. A number of THz lenses were reported to stimulate innovation in THz antenna design. Furthermore, research challenges for future multi-beam mmWave and THz antennas were elaborated. Research on multi-beam antennas for higher mmWave and THz frequencies is still limited because of the associated costs and technological challenges. This is currently true since most developments are targeting niche applications. With the growing interest in 6G and more generally B5G systems and their applications, it is expected that new innovations and designs for them will emerge in the coming decade in a manner similar to how lower mmWave technologies are currently expanding to meet mass market 5G applications.

REFERENCES

- [1] Y. J. Guo and R. W. Ziolkowski, *Advanced Antenna Array Engineering for 6G and Beyond Wireless Communications*. New York, NY, USA: Wiley, 2021.
- [2] W. Hong *et al.*, "Multibeam antenna technologies for 5G wireless communications," *IEEE Trans. Antennas Propag.*, vol. 65, no. 12, pp. 6231–6249, Dec. 2017.
- [3] B. Choudhury, A. R. Sonde, and R. M. Jha, "Terahertz antenna technology for space applications," in *Terahertz Antenna Technology for Space Applications*. Singapore: Springer, 2016, pp. 1–33.
- [4] S. U. Hwu, K. B. de Silva, and C. T. Jih, "Terahertz (THz) wireless systems for space applications," in *Proc. IEEE Sensors Appl. Symp.*, 2013, pp. 171–175.
- [5] Y. J. Guo, M. Ansari, and N. J. G. Fonseca, "Circuit type multiple beamforming networks for antenna arrays in 5G and 6G terrestrial and non-terrestrial networks," *IEEE J. Microw.*, vol. 1, no. 3, pp. 704–722, Jul. 2021, doi: [10.1109/JMW.2021.3072873](https://doi.org/10.1109/JMW.2021.3072873).
- [6] I. Ahmed *et al.*, "A survey on hybrid beamforming techniques in 5G: Architecture and system model perspectives," *IEEE Commun. Surveys Tuts.*, vol. 20, no. 4, pp. 3060–3097, 4th Quart., 2018.
- [7] J. O. Lodge and J. Howard, "On the concentration of electric radiation by lenses," *Nature*, vol. 40, no. 1, p. 94, 1889.
- [8] T. S. Bird, *Fundamentals of Aperture Antennas and Arrays: From Theory to Design, Fabrication and Testing*. Hoboken, NJ, USA: Wiley, 2015.
- [9] D. Archer, "Lens-fed multiple beam arrays," *Microw. J.*, vol. 27, p. 171, Sep. 1984.
- [10] Y. Li, L. Ge, M. Chen, Z. Zhang, Z. Li, and J. Wang, "Multibeam 3D-printed Luneburg lens fed by magnetoelectric dipole antennas for millimeter-wave MIMO applications," *IEEE Trans. Antennas Propag.*, vol. 67, no. 5, pp. 2923–2933, May 2019.
- [11] P. Liu, X.-W. Zhu, Y. Zhang, J. Li, and Z. Jiang, "3D-printed cylindrical Luneburg lens antenna for millimeter-wave applications," *Int. J. RF Microw. Comput. Aided Eng.*, vol. 30, no. 1, Jan. 2020, Art. no. e21994.
- [12] S. Matitsine, "Artificial dielectric material and method of manufacturing the same," U.S. Patent 8518537, Aug. 27, 2013.
- [13] C. Mateo-Segura, A. Dyke, H. Dyke, S. Haq, and Y. Hao, "Flat Luneburg lens via transformation optics for directive antenna applications," *IEEE Trans. Antennas Propag.*, vol. 62, no. 4, pp. 1945–1953, Apr. 2014.
- [14] Y. Su and Z. N. Chen, "A radial transformation-optics mapping for flat ultra-wide-angle dual-polarized stacked GRIN MTM Luneburg lens antenna," *IEEE Trans. Antennas Propag.*, vol. 67, no. 5, pp. 2961–2970, May 2019.

- [15] J. Ruze, "Wide-angle metal-plate optics," *Proc. IRE*, vol. 38, no. 1, pp. 53–59, Jan. 1950.
- [16] L.-Z. Song, P.-Y. Qin, S.-L. Chen, and Y. J. Guo, "An elliptical cylindrical shaped transmitarray for wide-angle multibeam applications," *IEEE Trans. Antennas Propag.*, early access, Jun. 5, 2021, doi: [10.1109/TAP.2021.3083828](https://doi.org/10.1109/TAP.2021.3083828).
- [17] S. A. Matos, E. B. Lima, J. R. Costa, C. A. Fernandes, and N. J. G. Fonseca, "Design of a 40 dBi planar bifocal lens for mechanical beam steering at Ka-band," in *Proc. 10th Eur. Conf. Antennas Propag. (EuCAP)*, Jun. 2016, pp. 1–4.
- [18] P. Nayeri, F. Yang, and A. Z. Elsherbeni, "Bifocal design and aperture phase optimizations of reflectarray antennas for wide-angle beam scanning performance," *IEEE Trans. Antennas Propag.*, vol. 61, no. 9, pp. 4588–4597, Sep. 2013.
- [19] E. B. Lima, S. A. Matos, J. R. Costa, C. A. Fernandes, and N. J. G. Fonseca, "Circular polarization wide-angle beam steering at Ka-band by in-plane translation of a plate lens antenna," *IEEE Trans. Antennas Propag.*, vol. 63, no. 12, pp. 5443–5455, Dec. 2015.
- [20] E. Martinez-de-Rioja, J. A. Encinar, R. Florencio, and C. Tienda, "3-D bifocal design method for dual-reflectarray configurations with application to multibeam satellite antennas in Ka-band," *IEEE Trans. Antennas Propag.*, vol. 67, no. 1, pp. 450–460, Jan. 2019.
- [21] F. Doucet *et al.*, "Analytical model and study of continuous parallel plate waveguide lens-like multiple-beam antennas," *IEEE Trans. Antennas Propag.*, vol. 66, no. 9, pp. 4426–4436, Sep. 2018.
- [22] N. J. G. Fonseca *et al.*, "Continuous parallel plate waveguide beam-former based on a bifocal constrained lens design," in *Proc. IEEE Int. Symp. Antennas Propag. (APSURSI)*, Oct. 2016, pp. 1347–1348.
- [23] F. Doucet *et al.*, "Shaped continuous parallel plate delay lens with enhanced scanning performance," *IEEE Trans. Antennas Propag.*, vol. 67, no. 11, pp. 6695–6704, Nov. 2019.
- [24] W. Rotman and R. Turner, "Wide-angle microwave lens for line source applications," *IEEE Trans. Antennas Propag.*, vol. AP-11, no. 6, pp. 623–632, Nov. 1963.
- [25] H. Gent, "The bootlace aerial," *Roy. Radar Establishment J.*, vol. 40, pp. 47–57, Oct. 1957.
- [26] J. Rao, "Multifocal three-dimensional bootlace lenses," *IEEE Trans. Antennas Propag.*, vol. AP-30, no. 6, pp. 1050–1056, Nov. 1982.
- [27] D. H. Archer and M. J. Maybell, "Rotman lens development history at Raytheon electronic warfare systems 1967–1995," in *Proc. IEEE Antennas Propag. Soc. Int. Symp.*, vol. 2, Dec. 2005, pp. 31–34.
- [28] D. Archer, R. Prickett, and C. Hartwig, "Multi-beam array antenna," U.S. Patent 3 761 936, Sep. 25, 1973.
- [29] D. H. Archer, "Radio frequency array antenna employing stacked parallel plate lenses," U.S. Patent 3 979 754, Sep. 7, 1976.
- [30] W. Lee, J. Kim, and Y. J. Yoon, "Compact two-layer Rotman lens-fed microstrip antenna array at 24 GHz," *IEEE Trans. Antennas Propag.*, vol. 59, no. 2, pp. 460–466, Feb. 2011.
- [31] M. S. Smith and A. K. S. Fong, "Amplitude performance of Ruze and Rotman lenses," *Radio Electron. Eng.*, vol. 53, no. 9, pp. 329–336, Sep. 1983.
- [32] M. S. Smith, "Multiple beam crossovers for a lens-fed antenna array," *J. Inst. Elect. Radio Eng.*, vol. 55, no. 1, pp. 33–36, Jan. 1985.
- [33] J.-W. Lian, Y.-L. Ban, H. Zhu, and Y. Guo, "Reduced-sidelobe multi-beam array antenna based on SIW Rotman lens," *IEEE Antennas Wireless Propag. Lett.*, vol. 29, no. 1, pp. 188–192, Dec. 2019, doi: [10.1109/LAWP.2019.2957509](https://doi.org/10.1109/LAWP.2019.2957509).
- [34] G. S. Hardie, R. Hernandez, and M. J. Maybell, "Parallel plate lens antenna," U.S. Patent 4 490 723, Dec. 25, 1984.
- [35] W. Wiebach and E. O. Rausch, "Improving the sidelobes of arrays fed by multiple-beam beam formers," in *Proc. IEEE Radar Conf. Challenges Radar Syst. Solutions (RADARCON)*, Aug. 1998, pp. 313–318.
- [36] F. Li, Y.-Z. Liu, and W. Huang, "A low sidelobe Rotman lens antenna feed by H-plane waveguide," in *Proc. IEEE CIE Int. Conf. Radar*, vol. 2, Mar. 2011, pp. 1197–1200.
- [37] D. Thomas, "Multiple beam synthesis of low sidelobe patterns in lens fed arrays," *IEEE Trans. Antennas Propag.*, vol. 26, no. 6, pp. 883–886, Nov. 1978.
- [38] N. J. G. Fonseca, "A focal curve design method for Rotman lenses with wider angular scanning range," *IEEE Antennas Wireless Propag. Lett.*, vol. 16, no. 4, pp. 54–57, Apr. 2016, doi: [10.1109/LAWP.2016.2554281](https://doi.org/10.1109/LAWP.2016.2554281).
- [39] E. Tolin, O. Litschke, S. Bruni, and F. Vipiana, "Compact extended scan range antenna array based on Rotman lens," *IEEE Trans. Antennas Propag.*, vol. 67, no. 12, pp. 7356–7367, Dec. 2019.
- [40] Y. F. Wu, Y. J. Cheng, and Z. X. Huang, "Ka-band near-field-focused 2-D steering antenna array with a focused Rotman lens," *IEEE Trans. Antennas Propag.*, vol. 66, no. 10, pp. 5204–5213, Oct. 2018.
- [41] S. Ershadi, A. Keshtkar, A. Bayat, A. Abdelrahman, and H. Xin, "Rotman lens design and optimization for 5G applications," *Int. J. Microw. Wireless Technol.*, vol. 10, no. 9, pp. 1048–1057, 2018.
- [42] A. Darvazehban, O. Manoochchri, M. A. Salari, P. Dehkoda, and A. Tavakoli, "Ultra-wideband scanning antenna array with Rotman lens," *IEEE Trans. Microw. Theory Techn.*, vol. 65, no. 9, pp. 3435–3442, Sep. 2017.
- [43] M. A. Hassanien, R. Hahnel, and D. Plettemeier, "Wideband Rotman lens beamforming technique for 5G wireless applications," in *Proc. IEEE 2nd Int. Conf. Comput. Appl. Inf. Security (ICCAIS)*, Jul. 2019, pp. 1–5.
- [44] N. Jastram and D. S. Filipovic, "Design of a wideband millimeter wave micromachined Rotman lens," *IEEE Trans. Antennas Propag.*, vol. 63, no. 6, pp. 2790–2796, Jun. 2015.
- [45] B.-H. Sun, Q.-Y. Liang, and G.-N. Zhou, "Miniaturized Rotman lens with applications to wireless communication," *Front. Inf. Technol. Electron. Eng.*, vol. 21, no. 1, pp. 144–158, Jan. 2020.
- [46] A. Attaran, R. Rashidzadeh, and A. Kouki, "60 GHz low phase error Rotman lens combined with wideband microstrip antenna array using LTCC technology," *IEEE Trans. Antennas Propag.*, vol. 64, no. 12, pp. 5172–5180, Dec. 2016.
- [47] K. Tekkoku, M. Ettore, L. Le Coq, and R. Sauleau, "Multibeam SIW slotted waveguide antenna system fed by a compact dual-layer Rotman lens," *IEEE Trans. Antennas Propag.*, vol. 64, no. 2, pp. 504–514, Feb. 2015.
- [48] K. Tekkoku, M. Ettore, and R. Sauleau, "SIW Rotman lens antenna with ridged delay lines and reduced footprint," *IEEE Trans. Microw. Theory Techn.*, vol. 66, no. 6, pp. 3136–3144, Jun. 2018.
- [49] K. Wu, M. Bozzi, and N. J. G. Fonseca, "Substrate integrated transmission lines: Review and applications," *IEEE J. Microw.*, vol. 1, no. 1, pp. 345–363, Jan. 2021.
- [50] Y. J. Cheng *et al.*, "Substrate integrated waveguide (SIW) Rotman lens and its Ka-band multibeam array antenna applications," *IEEE Trans. Antennas Propag.*, vol. 56, no. 8, pp. 2504–2513, Aug. 2008.
- [51] J.-W. Lian, Y.-L. Ban, and Y. J. Guo, "Wideband dual-layer Huygens' metasurface for high-gain multibeam array antennas," *IEEE Trans. Antennas Propag.*, early access, May 5, 2021, doi: [10.1109/TAP.2021.3076669](https://doi.org/10.1109/TAP.2021.3076669).
- [52] Y. Liu, H. Yang, Z. Jin, F. Zhao, and J. Zhu, "Compact Rotman lens-fed slot array antenna with low sidelobes," *IET Microw. Antennas Propag.*, vol. 12, no. 5, pp. 656–661, Dec. 2017.
- [53] Y. Liu, H. Yang, Z. Jin, F. Zhao, and J. Zhu, "A multibeam cylindrically conformal slot array antenna based on a modified Rotman lens," *IEEE Trans. Antennas Propag.*, vol. 66, no. 7, pp. 3441–3452, Jul. 2018.
- [54] Y. Gao, M. Khaliel, F. Zheng, and T. Kaiser, "Rotman lens based hybrid analog–digital beamforming in massive MIMO systems: Array architectures, beam selection algorithms and experiments," *IEEE Trans. Veh. Technol.*, vol. 66, no. 10, pp. 9134–9148, Oct. 2017.
- [55] M. A. B. Abbasi, V. F. Fusco, H. Tataria, and M. Matthaiou, "Lens-based beamformer for low-complexity millimeter-wave cellular systems," 2019. [Online]. Available: [arXiv:1902.08443](https://arxiv.org/abs/1902.08443).
- [56] M. A. B. Abbasi, H. Tataria, V. F. Fusco, and M. Matthaiou, "Performance of a 28 GHz two-stage Rotman lens beamformer for millimeter wave cellular systems," in *Proc. IEEE 13th Eur. Conf. Antennas Propag. (EuCAP)*, Jun. 2019, pp. 1–4.
- [57] T. K. V. Dai, T. Nguyen, and O. Kilib, "Compact multi-layer microstrip Rotman lens design using coupling slots to support millimeter wave devices," *IET Microw. Antennas Propag.*, vol. 12, no. 8, pp. 1260–1265, Aug. 2018.
- [58] K. V. Hoel, S. Kristoffersen, N. Jastram, and D. S. Filipovic, "3D printed Rotman lens," in *Proc. 47th Eur. Microw. Conf. (EuMC)*, Dec. 2017, pp. 125–128.
- [59] S.-A. Gomanne *et al.*, "Comparative study of waveguide rotman lens designs for Q/V band applications," in *Proc. 40th ESA Antenna Workshop*, Noordwijk, The Netherlands, Oct. 2019, pp. 1–5.
- [60] R. K. Luneburg, *Mathematical Theory of Optics*. Providence, RI, USA: Univ. California Press, 1964.

- [61] C. A. Fernandes, E. B. Lima, and J. R. Costa, "Dielectric lens antennas," in *Handbook of Antenna Technology*. Singapore: Springer, 2016, pp. 1001–1064.
- [62] Y. J. Guo and B. Jones, "Base station antennas," in *Antenna Engineering Handbook*, J. Volakis, Ed. London, U.K.: McGraw-Hill, 2018, ch. 40.
- [63] M. Ansari, B. Jones, H. Zhu, N. Shariati, and Y. J. Guo, "A highly efficient spherical Luneburg lens for low microwave frequencies realized with a metal-based artificial medium," *IEEE Trans. Antennas Propag.*, early access, 2021, doi: [10.1109/TAP.2020.3044638](https://doi.org/10.1109/TAP.2020.3044638).
- [64] J. Li *et al.*, "Design of a broadband metasurface Luneburg lens for full-angle operation," *IEEE Trans. Antennas Propag.*, vol. 67, no. 4, pp. 2442–2451, Apr. 2019.
- [65] J. Pourahmadazar and T. A. Denidni, "Towards millimeter-wavelength: Transmission-mode Fresnel-zone plate lens antennas using plastic material porosity control in homogeneous medium," *Sci. Rep.*, vol. 8, no. 1, pp. 1–14, Jan. 2018.
- [66] A. Demetriadou and Y. Hao, "A grounded slim Luneburg lens antenna based on transformation electromagnetics," *IEEE Antennas Wireless Propag. Lett.*, vol. 10, no. 12, pp. 1590–1593, Dec. 2011.
- [67] O. Zetterstrom, N. J. G. Fonseca, and O. Quevedo-Teruel, "Compressed lenses via transformation optics for mobile satellite communications," in *Proc. 14th Eur. Conf. Antennas Propag. (EuCAP)*, Jul. 2020, pp. 1–3.
- [68] A. Demetriadou and Y. Hao, "Slim Luneburg lens for antenna applications," *Opt. Exp.*, vol. 19, no. 21, pp. 19925–19934, 2011.
- [69] A. Alex-Amor *et al.*, "Glide-symmetric metallic structures with elliptical holes for lens compression," *IEEE Trans. Microw. Theory Techn.*, vol. 68, no. 10, pp. 4236–4248, Oct. 2020.
- [70] J.-M. Poyanco, O. Zetterstrom, P. Castillo-Tapia, N. J. Fonseca, F. Pizarro, and O. Quevedo-Teruel, "Two-dimensional glide-symmetric dielectric structures for planar graded-index lens antennas," *IEEE Antennas Wireless Propag. Lett.*, early access, Jun. 21, 2021, doi: [10.1109/LAWP.2021.3092169](https://doi.org/10.1109/LAWP.2021.3092169).
- [71] H.-T. Chou and Z.-D. Yan, "Parallel-plate Luneburg lens antenna for broadband multibeam radiation at millimeter-wave frequencies with design optimization," *IEEE Trans. Antennas Propag.*, vol. 66, no. 11, pp. 5794–5804, Nov. 2018.
- [72] C. Hua, X. Wu, N. Yang, and W. Wu, "Air-filled parallel-plate cylindrical modified Luneburg lens antenna for multiple-beam scanning at millimeter-wave frequencies," *IEEE Trans. Microw. Theory Techn.*, vol. 61, no. 1, pp. 436–443, Jan. 2013.
- [73] A. B. Numan, J.-F. Frigon, and J.-J. Laurin, "Printed W-band multi-beam antenna with Luneburg lens-based beamforming network," *IEEE Trans. Antennas Propag.*, vol. 66, no. 10, pp. 5614–5619, Oct. 2018.
- [74] C. Wang, J. Wu, and Y.-X. Guo, "A 3D-printed wideband circularly polarized parallel-plate Luneburg lens antenna," *IEEE Trans. Antennas Propag.*, vol. 68, no. 6, pp. 4944–4949, Jun. 2020.
- [75] P. Liu *et al.*, "A novel E-plane-focused cylindrical Luneburg lens loaded with metal grids for side lobe level reduction," *IEEE Trans. Antennas Propag.*, vol. 68, no. 2, pp. 736–744, Feb. 2020.
- [76] A. Boriskin, A. Vorobyov, and R. Sauleau, "Two-shell radially symmetric dielectric lenses as low-cost analogs of the Luneburg lens," *IEEE Trans. Antennas Propag.*, vol. 59, no. 8, pp. 3089–3093, Aug. 2011.
- [77] B. Fuchs *et al.*, "Design optimization of multishell Luneburg lenses," *IEEE Trans. Antennas Propag.*, vol. 55, no. 2, pp. 283–289, Feb. 2007.
- [78] A. N. Korotkov, S. N. Shabunin, and V. A. Chechetkin, "The cylindrical Luneburg lens discretization influence on its radiation parameters," in *Proc. Int. Multi Conf. Eng. Comput. Inf. Sci. (SIBIRCON)*, Sep. 2017, pp. 394–398.
- [79] S. Rondineau, M. Himdi, and J. Sorieux, "A sliced spherical Luneburg lens," *IEEE Antennas Wireless Propag. Lett.*, vol. 2, pp. 163–166, 2003.
- [80] H. F. Ma *et al.*, "Three-dimensional gradient-index materials and their applications in microwave lens antennas," *IEEE Trans. Antennas Propag.*, vol. 61, no. 5, pp. 2561–2569, May 2013.
- [81] H. F. Ma and T. J. Cui, "Three-dimensional broadband and broad-angle transformation-optics lens," *Nat. Commun.*, vol. 1, no. 1, pp. 1–7, Jan. 2010.
- [82] J. Ruiz-García, E. Martini, C. D. Giovampaola, D. González-Ovejero, and S. Maci, "Reflecting Luneburg lenses," *IEEE Trans. Antennas Propag.*, early access, 2021, doi: [10.1109/TAP.2020.3044668](https://doi.org/10.1109/TAP.2020.3044668).
- [83] K. F. Brakora, J. Halloran, and K. Sarabandi, "Design of 3D monolithic MMW antennas using ceramic stereolithography," *IEEE Trans. Antennas Propag.*, vol. 55, no. 3, pp. 790–797, Mar. 2007.
- [84] K. Liu, S. Yang, S. Qu, Y. Chen, and J. Hu, "2D flat Luneburg lens antenna for multibeam scanning application," *Electron. Lett.*, vol. 55, no. 25, pp. 1317–1318, 2019.
- [85] N. Kundtz and D. R. Smith, "Extreme-angle broadband metamaterial lens," *Nat. Mater.*, vol. 9, no. 2, pp. 129–132, Feb. 2010.
- [86] Y. Amarasinghe *et al.*, "Broadband wide-angle terahertz antenna based on the application of transformation optics to a Luneburg lens," *Sci. Rep.*, vol. 11, no. 1, pp. 1–8, Mar. 2021.
- [87] J. Ruiz-García, E. Martini, C. D. Giovampaola, D. González-Ovejero, and S. Maci, "Reflecting Luneburg lenses," *IEEE Trans. Antennas Propag.*, early access, Dec. 21, 2020, doi: [10.1109/TAP.2020.3044668](https://doi.org/10.1109/TAP.2020.3044668).
- [88] A. Gutman, "Modified Luneburg lens," *J. Appl. Phys.*, vol. 25, no. 7, pp. 855–859, Jul. 1954.
- [89] O. Bjorkqvist, O. Zetterstrom, and O. Quevedo-Teruel, "Additive manufactured dielectric Gutman lens," *Electron. Lett.*, vol. 55, no. 25, pp. 1318–1320, Dec. 2019.
- [90] R. F. Rinehart, "A solution of the problem of rapid scanning for radar antennae," *J. Appl. Phys.*, vol. 19, no. 9, pp. 860–862, Sep. 1948.
- [91] R. Rinehart, "A family of designs for rapid scanning radar antennas," *Proc. IRE*, vol. 40, no. 6, pp. 686–688, Jun. 1952.
- [92] Q. Liao, N. J. G. Fonseca, and O. Quevedo-Teruel, "Compact multibeam fully metallic geodesic Luneburg lens antenna based on Non-Euclidean transformation optics," *IEEE Trans. Antennas Propag.*, vol. 66, no. 12, pp. 7383–7388, Dec. 2018.
- [93] N. J. G. Fonseca, Q. Liao, and O. Quevedo-Teruel, "Equivalent planar lens ray-tracing model to design modulated geodesic lenses using non-euclidean transformation optics," *IEEE Trans. Antennas Propag.*, vol. 68, no. 5, pp. 3410–3422, May 2020.
- [94] N. J. G. Fonseca, Q. Liao, and O. Quevedo-Teruel, "Compact parallel-plate waveguide half-Luneburg geodesic lens in the K-band," *IET Microw. Antennas Propag.*, vol. 15, no. 2, pp. 123–130, Feb. 2021.
- [95] N. J. G. Fonseca, "The water drop lens: Revisiting the past to shape the future," *EurAAP Rev. Electromag.*, to be published.
- [96] D. McGrath, "Planar three-dimensional constrained lenses," *IEEE Trans. Antennas Propag.*, vol. AP-34, no. 1, pp. 46–50, Jan. 1986.
- [97] J. R. Reis, M. Vala, and R. F. Caldeirinha, "Review paper on transmitarray antennas," *IEEE Access*, vol. 7, pp. 94171–94188, 2019.
- [98] Q. Chen, Y. Saifullah, G.-M. Yang, and Y.-Q. Jin, "Electronically reconfigurable unit cell for transmit-reflect-arrays in the X-band," *Opt. Exp.*, vol. 29, no. 2, pp. 1470–1480, Feb. 2021.
- [99] J. Y. Lau and S. V. Hum, "Analysis and characterization of a multipole reconfigurable transmitarray element," *IEEE Trans. Antennas Propag.*, vol. 59, no. 1, pp. 70–79, Jan. 2010.
- [100] L. Di Palma, "Reconfigurable transmitarray antennas at millimeter-wave frequencies," Ph.D. dissertation, Dept. Elect. Eng., Université Rennes 1, Rennes, France, 2015.
- [101] J. R. Reis *et al.*, "FSS-inspired transmitarray for two-dimensional antenna beamsteering," *IEEE Trans. Antennas Propag.*, vol. 64, no. 6, pp. 2197–2206, Jun. 2016.
- [102] N. Kou, S. Yu, Z. Ding, and Z. Zhang, "One-dimensional beam scanning transmitarray lens antenna fed by microstrip linear array," *IEEE Access*, vol. 7, pp. 90731–90740, 2019.
- [103] Z.-W. Miao *et al.*, "140 GHz high-gain LTCC-integrated transmitarray antenna using a wideband SIW aperture-coupling phase delay structure," *IEEE Trans. Antennas Propag.*, vol. 66, no. 1, pp. 182–190, Jan. 2017.
- [104] X. Liu *et al.*, "Ultra-broadband all dielectric transmitarray designing based on genetic algorithm optimization and 3D print technology," *IEEE Trans. Antennas Propag.*, vol. 69, no. 4, pp. 2003–2012, Apr. 2021.
- [105] Y. Xiao, F. Yang, S. Xu, M. Li, K. Zhu, and H. Sun, "Design and implementation of a wideband 1-bit transmitarray based on a Yagi-Vivaldi unit cell," *IEEE Trans. Antennas Propag.*, early access, Jan. 8, 2021, doi: [10.1109/TAP.2020.3048496](https://doi.org/10.1109/TAP.2020.3048496).

- [106] C. Jouanlanne *et al.*, "Wideband linearly polarized transmitarray antenna for 60 GHz backhauling," *IEEE Trans. Antennas Propag.*, vol. 65, no. 3, pp. 1440–1445, Mar. 2017.
- [107] C. Tian, Y. Jiao, G. Zhao, and H. Wang, "A wideband transmitarray using triple-layer elements combined with cross slots and double square rings," *IEEE Antennas Wireless Propag. Lett.*, vol. 16, no. 1, pp. 1561–1564, Jan. 2017.
- [108] R. Y. Wu, Y. B. Li, W. Wu, C. B. Shi, and T. J. Cui, "High-gain dual-band transmitarray," *IEEE Trans. Antennas Propag.*, vol. 65, no. 7, pp. 3481–3488, Jul. 2017.
- [109] S. A. Matos *et al.*, "High gain dual-band beam-steering transmit array for satcom terminals at Ka-band," *IEEE Trans. Antennas Propag.*, vol. 65, no. 7, pp. 3528–3539, Jul. 2017.
- [110] S. Yang, Z. Yan, T. Zhang, M. Cai, F. Fan, and X. Li, "Multifunctional tri-band dual-polarized antenna combining transmitarray and reflectarray," *IEEE Trans. Antennas Propag.*, early access, Feb. 26, 2021, doi: [10.1109/TAP.2021.3060938](https://doi.org/10.1109/TAP.2021.3060938).
- [111] P. Naseri, S. A. Matos, E. B. Lima, J. R. Costa, C. A. Fernandes, and N. J. G. Fonseca, "Efficient evaluation of gradient transmit-arrays through an equivalent dispersive dielectric description," *IEEE Trans. Antennas Propag.*, vol. 67, no. 9, pp. 5997–6007, Sep. 2019.
- [112] A. Barka, S. A. Matos, J. R. Costa, C. A. Fernandes, and H. Chreim, "Applying massively parallel computing to multiscale Ka dual-band transmit-array analysis using FETI-2LM," *IEEE J. Multiscale Multiphys. Comput. Tech.*, vol. 5, no. 10, pp. 235–244, Oct. 2020.
- [113] G. Liu, M. R. D. Kodnoeih, K. T. Pham, E. M. Cruz, D. González-Ovejero, and R. Sauleau, "A millimeter-wave multibeam transparent transmitarray antenna at Ka-band," *IEEE Antennas Wireless Propag. Lett.*, vol. 18, no. 4, pp. 631–635, Apr. 2019.
- [114] A. H. Abdelrahman *et al.*, "Analysis and design of transmitarray antennas," *Synth. Lectures Antennas*, vol. 6, no. 1, pp. 1–175, Jan. 2017.
- [115] A. H. Abdelrahman, A. Z. Elsherbeni, and F. Yang, "High-gain and broadband transmitarray antenna using triple-layer spiral dipole elements," *IEEE Antennas Wireless Propag. Lett.*, vol. 13, no. 7, pp. 1288–1291, Jul. 2014.
- [116] P.-Y. Feng, S.-W. Qu, S. Yang, L. Shen, and J. Zhao, "Ku-band transmitarrays with improved feed mechanism," *IEEE Trans. Antennas Propag.*, vol. 66, no. 6, pp. 2883–2891, Jun. 2018.
- [117] L.-Z. Song, P.-Y. Qin, S.-L. Chen, and Y. J. Guo, "A high-efficiency conformal transmitarray antenna employing dual-layer ultrathin Huygens element," *IEEE Trans. Antennas Propag.*, vol. 69, no. 2, pp. 848–858, Feb. 2021.
- [118] P.-Y. Qin, L.-Z. Song, and Y. J. Guo, "Beam steering conformal transmitarray employing ultra-thin triple-layer slot elements," *IEEE Trans. Antennas Propag.*, vol. 67, no. 8, pp. 5390–5398, Aug. 2019.
- [119] J. R. Reis, R. F. S. Caldeirinha, A. Hammoudeh, and N. Copner, "Electronically reconfigurable FSS-inspired transmitarray for 2D beamsteering," *IEEE Trans. Antennas Propag.*, vol. 65, no. 9, pp. 4880–4885, Sep. 2017.
- [120] L. Di Palma, A. Clemente, L. Dussot, R. Sauleau, P. Potier, and P. Pouliquen, "Circularly-polarized reconfigurable transmitarray in Ka-band with beam scanning and polarization switching capabilities," *IEEE Trans. Antennas Propag.*, vol. 65, no. 2, pp. 529–540, Feb. 2017.
- [121] F. F. Manzillo, A. Clemente, and J. L. González-Jiménez, "High-gain D-band transmitarrays in standard PCB technology for beyond-5G communications," *IEEE Trans. Antennas Propag.*, vol. 68, no. 1, pp. 587–592, Jan. 2020.
- [122] S. H. Lee *et al.*, "Switching terahertz waves with gate-controlled active graphene metamaterials," *Nat. Mater.*, vol. 11, no. 11, pp. 936–941, Nov. 2012.
- [123] C. N. Alvarez, R. Cheung, and J. S. Thompson, "Performance analysis of hybrid metal-graphene frequency reconfigurable antennas in the microwave regime," *IEEE Trans. Antennas Propag.*, vol. 65, no. 4, pp. 1558–1569, Apr. 2017.
- [124] W. Yao, L. Tang, J. Wang, C. Ji, X. Wei, and Y. Jiang, "Spectrally and spatially tunable terahertz metasurface lens based on graphene surface plasmons," *IEEE Photon. J.*, vol. 10, no. 4, pp. 1–8, Apr. 2018.
- [125] S. Qu and H. Yi, "Low-cost two-layer terahertz transmitarray," in *Proc. Int. Appl. Comput. Electromagn. Soc. Symp. (ACES)*, Sep. 2017, pp. 1–2.
- [126] A. S. Dunbar, "Calculation of doubly curved reflectors for shaped beams," *Proc. IRE*, vol. 36, no. 10, pp. 1289–1296, Oct. 1948.
- [127] A. Brunner, "Possibilities of dimensioning doubly curved reflectors for azimuth-search radar antennas," *IEEE Trans. Antennas Propag.*, vol. AP-19, no. 1, pp. 52–57, Jan. 1971.
- [128] N. J. G. Fonseca, E. Girard, and H. Legay, "Doubly curved reflector design for hybrid array fed reflector antennas," *IEEE Trans. Antennas Propag.*, vol. 66, no. 4, pp. 2079–2083, Apr. 2018.
- [129] W. V. T. Rusch, A. Prata, Y. Rahmat-Samii, and R. A. Shore, "Derivation and application of the equivalent paraboloid for classical offset cassegrain and gregorian antennas," *IEEE Trans. Antennas Propag.*, vol. 38, no. 8, pp. 1141–1149, Aug. 1990.
- [130] Y. J. Cheng, W. Hong, and K. Wu, "Millimeter-wave substrate integrated waveguide multibeam antenna based on the parabolic reflector principle," *IEEE Trans. Antennas Propag.*, vol. 56, no. 9, pp. 3055–3058, Sep. 2008.
- [131] W. Rotman, "Wide-angle scanning with microwave double-layer pillboxes," *IRE Trans. Antennas Propag.*, vol. 6, no. 1, pp. 96–105, Jan. 1958.
- [132] Z. L. Ma and C. H. Chan, "A novel surface-wave-based high-impedance surface multibeam antenna with full azimuth coverage," *IEEE Trans. Antennas Propag.*, vol. 65, no. 4, pp. 1579–1588, Apr. 2017.
- [133] E. Gandini, M. Ettore, M. Casaletti, K. Tekkoku, L. Le Coq, and R. Sauleau, "SIW slotted waveguide array with pillbox transition for mechanical beam scanning," *IEEE Antennas Wireless Propag. Lett.*, vol. 11, no. 12, pp. 1572–1575, Nov. 2012, doi: [10.1109/LAWP.2012.2235057](https://doi.org/10.1109/LAWP.2012.2235057).
- [134] M. Ettore, F. F. Manzillo, M. Casaletti, R. Sauleau, L. Le Coq, and N. Capet, "Continuous transverse stub array for Ka-band applications," *IEEE Trans. Antennas Propag.*, vol. 63, no. 11, pp. 4792–4800, Nov. 2015.
- [135] M. Ettore, R. Sauleau, and L. Le Coq, "Multi-beam multi-layer leaky-wave SIW pillbox antenna for millimeter-wave applications," *IEEE Trans. Antennas Propag.*, vol. 59, no. 4, pp. 1093–1100, Apr. 2011.
- [136] F. F. Manzillo *et al.*, "A wide-angle scanning switched-beam antenna system in LTCC technology with high beam crossing levels for V-band communications," *IEEE Trans. Antennas Propag.*, vol. 67, no. 1, pp. 541–553, Jan. 2019.
- [137] K. Tekkoku, M. Ettore, L. Le Coq, and R. Sauleau, "SIW pillbox antenna for monopulse radar applications," *IEEE Trans. Antennas Propag.*, vol. 63, no. 9, pp. 3918–3927, Sep. 2015.
- [138] K. Tekkoku, M. Ettore, and R. Sauleau, "Multibeam pillbox antenna integrating amplitude-comparison monopulse technique in the 24 GHz band for tracking applications," *IEEE Trans. Antennas Propag.*, vol. 66, no. 5, pp. 2616–2621, May 2018.
- [139] S. Stein, "On cross coupling in multiple-beam antennas," *IRE Trans. Antennas Propag.*, vol. 10, no. 5, pp. 548–557, Sep. 1962.
- [140] K. Tekkoku, M. Ettore, E. Gandini, and R. Sauleau, "Multibeam pillbox antenna with low sidelobe level and high-beam crossover in SIW technology using the split aperture decoupling method," *IEEE Trans. Antennas Propag.*, vol. 63, no. 11, pp. 5209–5215, Nov. 2015.
- [141] S.-P. Yan, M.-H. Zhao, Y.-L. Ban, J.-W. Lian, and Z. Nie, "Dual-layer SIW multibeam pillbox antenna with reduced sidelobe level," *IEEE Antennas Wireless Propag. Lett.*, vol. 18, no. 3, pp. 541–545, Mar. 2019.
- [142] M. Ettore, A. Neto, G. Gerini, and S. Maci, "Leaky-wave slot array antenna fed by a dual reflector system," *IEEE Trans. Antennas Propag.*, vol. 56, no. 10, pp. 3143–3149, Oct. 2008.
- [143] J.-W. Lian, Y.-L. Ban, Z. Chen, B. Fu, and C. Xiao, "SIW folded cassegrain lens for millimeter-wave multibeam application," *IEEE Antennas Wireless Propag. Lett.*, vol. 17, no. 4, pp. 583–586, Apr. 2018.
- [144] A. N. Plastikov, "A high-gain multibeam bifocal reflector antenna with 40° field of view for satellite ground station applications," *IEEE Trans. Antennas Propag.*, vol. 64, no. 7, pp. 3251–3254, Jul. 2016.
- [145] A. Hosseini, S. Kabiri, and F. De Flaviis, "V-band high-gain printed quasi-parabolic reflector antenna with beam-steering," *IEEE Trans. Antennas Propag.*, vol. 65, no. 4, pp. 1589–1598, Apr. 2017.
- [146] D. Berry, R. Malech, and W. Kennedy, "The reflectarray antenna," *IEEE Trans. Antennas Propag.*, vol. AP-11, no. 6, pp. 645–651, Nov. 1963.
- [147] J. Huang, "Reflectarray antenna," in *Encyclopedia of RF and Microwave Engineering*. Hoboken, NJ, USA: Wiley, 2005.

- [148] Y. Rahmat-Samii and R. Haupt, "Reflector antenna developments: A perspective on the past, present and future," *IEEE Antennas Propag. Mag.*, vol. 57, no. 2, pp. 85–95, Apr. 2015.
- [149] S. Dang, O. Amin, B. Shihada, and M.-S. Alouini, "What should 6G be?" *Nat. Electron.*, vol. 3, no. 1, pp. 20–29, Jan. 2020.
- [150] W. Saad, M. Bennis, and M. Chen, "A vision of 6G wireless systems: Applications, trends, technologies, and open research problems," *IEEE Netw.*, vol. 34, no. 3, pp. 134–142, Mar. 2019.
- [151] X. You *et al.*, "Towards 6G wireless communication networks: Vision, enabling technologies, and new paradigm shifts," *Sci. China Inf. Sci.*, vol. 64, no. 1, pp. 1–74, Jan. 2021.
- [152] I. Mehdi, J. Siles, C. P. Chen, and J. M. Jornet, "THz technology for space communications," in *Proc. IEEE Asia-Pac. Microw. Conf. (APMC)*, Jan. 2018, pp. 76–78.
- [153] D. Pasqualini and S. Maci, "High-frequency analysis of integrated dielectric lens antennas," *IEEE Trans. Antennas Propag.*, vol. 52, no. 3, pp. 840–847, Mar. 2004.
- [154] X. Gao, T. Zhang, J. Du, and Y. J. Guo, "340 GHz double-sideband mixer based on antenna-coupled high-temperature superconducting Josephson junction," *IEEE Trans. THz Sci. Technol.*, vol. 10, no. 1, pp. 21–31, Jan. 2019.
- [155] J. R. Costa, C. A. Fernandes, G. Godi, R. Sauleau, L. Le Coq, and H. Legay, "Compact Ka-band lens antennas for LEO satellites," *IEEE Trans. Antennas Propag.*, vol. 56, no. 5, pp. 1251–1258, May 2008.
- [156] J. R. Costa, E. B. Lima, and C. A. Fernandes, "Compact beam-steerable lens antenna for 60-GHz wireless communications," *IEEE Trans. Antennas Propag.*, vol. 57, no. 10, pp. 2926–2933, Oct. 2009.
- [157] D. F. Filipovic, S. S. Gearhart, and G. M. Rebeiz, "Double-slot antennas on extended hemispherical and elliptical silicon dielectric lenses," *IEEE Trans. Microwave Theory Techn.*, vol. 41, no. 10, pp. 1738–1749, Oct. 1993.
- [158] G. M. Rebeiz, "Millimeter-wave and terahertz integrated circuit antennas," *Proc. IEEE*, vol. 80, no. 11, pp. 1748–1770, Nov. 1992.
- [159] K. Konstantinidis *et al.*, "Low-THz dielectric lens antenna with integrated waveguide feed," *IEEE Trans. THz Sci. Technol.*, vol. 7, no. 5, pp. 572–581, Sep. 2017.
- [160] M. Alonso-delPino, C. Jung-Kubiak, T. Reck, N. Llombart, and G. Chattopadhyay, "Beam scanning of silicon lens antennas using integrated piezomotors at submillimeter wavelengths," *IEEE Trans. THz Sci. Technol.*, vol. 9, no. 1, pp. 47–54, Jan. 2019.
- [161] D. G. Bodnar, "Lens antennas," in *The Handbook of Antenna Design*, vol. 1. London, U.K.: Peter Peregrinus, 1986, pp. 1–31.
- [162] A. Artemenko, A. Maltsev, A. Mozharovskiy, A. Sevastyanov, V. Ssorin, and R. Maslennikov, "Millimeter-wave electronically steerable integrated lens antennas for WLAN/WPAN applications," *IEEE Trans. Antennas Propag.*, vol. 61, no. 4, pp. 1665–1671, Apr. 2012.
- [163] A. A. Artemenko, V. N. Ssorin, R. O. Maslennikov, and A. V. Mozharovskiy, "Lens antenna with electronic beam steering capabilities," U.S. Patent App. 14 593 552, Apr. 30, 2015.
- [164] A. Artemenko, A. Mozharovskiy, A. Maltsev, R. Maslennikov, A. Sevastyanov, and V. Ssorin, "Experimental characterization of E-band two-dimensional electronically beam-steerable integrated lens antennas," *IEEE Antennas Wireless Propag. Lett.*, vol. 1, no. 2, pp. 1188–1191, Dec. 2013, doi: [10.1109/LAWP.2013.2282212](https://doi.org/10.1109/LAWP.2013.2282212).
- [165] X. Wei *et al.*, "Generation of arbitrary order Bessel beams via 3D printed axicons at the terahertz frequency range," *Appl. Opt.*, vol. 54, no. 36, pp. 10641–10649, 2015.
- [166] W. D. Furlan, V. Ferrando, J. A. Monsoriu, P. Zagrajek, E. Czerwińska, and M. Szustakowski, "3D printed diffractive terahertz lenses," *Opt. Lett.*, vol. 41, no. 8, pp. 1748–1751, Aug. 2016.
- [167] H. Yi, S.-W. Qu, K.-B. Ng, C. H. Chan, and X. Bai, "3-D printed millimeter-wave and terahertz lenses with fixed and frequency scanned beam," *IEEE Trans. Antennas Propag.*, vol. 64, no. 2, pp. 442–449, Feb. 2016.
- [168] K. X. Wang and H. Wong, "A wideband millimeter-wave circularly polarized antenna with 3D printed polarizer," *IEEE Trans. Antennas Propag.*, vol. 65, no. 3, pp. 1038–1046, Mar. 2017.
- [169] G. B. Wu, Y.-S. Zeng, K. F. Chan, S.-W. Qu, and C. H. Chan, "High-gain circularly polarized lens antenna for terahertz applications," *IEEE Antennas Wireless Propag. Lett.*, vol. 18, no. 5, pp. 921–925, May 2019.
- [170] G.-B. Wu, Y.-S. Zeng, K. F. Chan, S.-W. Qu, and C. H. Chan, "3-D printed circularly polarized modified Fresnel lens operating at terahertz frequencies," *IEEE Trans. Antennas Propag.*, vol. 67, no. 7, pp. 4429–4437, Jul. 2019.
- [171] Y. J. Guo and S. K. Barton, *Fresnel Zone Antennas*. New York, NY, USA: Springer, 2013.
- [172] L.-Z. Song, P.-Y. Qin, S. Maci, and Y. J. Guo, "Ultrawideband conformal transmitarray employing connected slot-bowtie elements," *IEEE Trans. Antennas Propag.*, vol. 69, no. 6, pp. 3273–3283, Jun. 2021.
- [173] D. González-Ovejero, G. Minatti, G. Chattopadhyay, and S. Maci, "Multibeam by metasurface antennas," *IEEE Trans. Antennas Propag.*, vol. 65, no. 6, pp. 2923–2930, Jun. 2017.



Y. JAY GUO (Fellow, IEEE) received the bachelor's and master's degrees from Xidian University, China, in 1982 and 1984, respectively, and the Ph.D. degree from Xian Jiaotong University, China, in 1987.

He is a Distinguished Professor and the Director of Global Big Data Technologies Centre, University of Technology Sydney, Australia. Prior to this appointment in 2014, he served as a Director of CSIRO for over nine years. Before joining CSIRO, he held various senior technology leadership positions with Fujitsu, Siemens, and NEC, U.K. He has published over 550 research papers including 280 journal papers, most of which are in IEEE transactions, and he holds 26 patents. His research interest includes antennas, mmWave and THz communications, and sensing systems as well as big data technologies.

Dr. Guo has won a number of most prestigious Australian Engineering Excellence Awards in 2007 and 2012, and CSIRO Chairman's Medal in 2007 and 2012. He was named one of the most influential engineers in Australia in 2014 and 2015, and one of the top researchers in Australia in 2020. He has chaired numerous international conferences and served as guest editors for a number of IEEE publications. He is the Chair of International Steering Committee, International Symposium on Antennas and Propagation. He was the International Advisory Committee Chair of IEEE VTC2017, a General Chair of ISAP2022, ISAP2015, iWAT2014, and WPMC'2014, and a TPC Chair of 2010 IEEE WCNC, and 2012 and 2007 IEEE ISCTI. He served as a Guest Editor of special issues on "Antennas for Satellite Communications" and "Antennas and Propagation Aspects of 60-90GHz Wireless Communications," both in IEEE TRANSACTIONS ON ANTENNAS AND PROPAGATION, Special Issue on "Communications Challenges and Dynamics for Unmanned Autonomous Vehicles," IEEE JOURNAL ON SELECTED AREAS IN COMMUNICATIONS, and Special Issue on "5G for Mission Critical Machine Communications," *IEEE Network Magazine*. He is a Fellow of the Australian Academy of Engineering and Technology and IET, and was a member of the College of Experts of Australian Research Council (ARC, 2016–2018).



MARAL ANSARI (Student Member, IEEE) received the M.S. degree (Hons.) in electrical and communication engineering from Tabriz University, Tabriz, Iran, in 2015. She is currently pursuing the Ph.D. degree in electrical engineering with the Global Big Data Technologies Center, School of Electrical and Data Engineering, Faculty of Engineering and IT, University of Technology Sydney, Ultimo, NSW, Australia. Her current research interests include multibeam antenna arrays, lens antennas, mmWave beam scanning, and beamforming networks.



RICHARD W. ZIOLKOWSKI (Life Fellow, IEEE) received the B.Sc. (*magna cum laude*) degree (Hons.) in physics from Brown University, Providence, RI, USA, in 1974, the M.S. and Ph.D. degrees in physics from the University of Illinois at Urbana–Champaign, Urbana, IL, USA, in 1975 and 1980, respectively, and the Honorary Doctorate degree from the Technical University of Denmark, Kongens Lyngby, Denmark, in 2012.

He is currently a Distinguished Professor with the Global Big Data Technologies Centre, Faculty of Engineering and Information Technologies, University of Technology Sydney, Ultimo, NSW, Australia. He became a Professor Emeritus with the University of Arizona in 2018, where he was a Litton Industries John M. Leonis Distinguished Professor with the Department of Electrical and Computer Engineering, College of Engineering and was also a Professor with the College of Optical Sciences. He was the Computational Electronics and Electromagnetics Thrust Area Leader with the Engineering Research Division, Lawrence Livermore National Laboratory before joining The University of Arizona, Tucson, AZ, USA, in 1990. His current research interests include the application of new mathematical and numerical methods to linear and nonlinear problems dealing with the interaction of electromagnetic and acoustic waves with complex linear and nonlinear media, as well as metamaterials, metamaterial-inspired structures, nano-structures, and other classical and quantum applications-specific configurations.

Prof. Ziolkowski was the recipient of the 2019 IEEE Electromagnetics Award (IEEE Technical Field Award). He served as the President of the IEEE Antennas and Propagation Society (AP-S) in 2005 and has had many other AP-S leadership roles. He is also actively involved with the URSI, EurAAP, OSA, and SPIE professional societies. He was the 2014–2015 Australian DSTO Fulbright Distinguished Chair in Advanced Science and Technology. He was a 2014 Thomas-Reuters Highly Cited Researcher. He is a Fellow of the Optical Society of America (OSA, 2006) and the American Physical Society (2016).



NELSON J. G. FONSECA (Senior Member, IEEE) received the M.Eng. degree in electrical engineering from Ecole Nationale Supérieure d'Electrotechnique, Electronique, Informatique, Hydraulique et Télécommunications, Toulouse, France, in 2003, the M.Sc. degree in electrical engineering from the Ecole Polytechnique de Montreal, Montreal, QC, Canada, in 2003, and the Ph.D. degree in electrical engineering from Institut National Polytechnique de Toulouse—Université de Toulouse, France, in 2010.

He currently works as an Antenna Engineer with the Antenna and Sub-Millimetre Waves Section, European Space Agency (ESA), Noordwijk, The Netherlands. Since November 2020, he has held an Honorary Appointment as a Professional Fellow with the University of Technology Sydney, Australia. He has authored or coauthored more than 230 papers in peer-reviewed journals and conferences and has over 50 patents issued or pending. His research interests include multiple beam antennas for space missions, beam-former theory and design, ground terminal antennas, transfer of technology from and to terrestrial systems, including 5G networks and novel manufacturing techniques.

Dr. Fonseca received several prizes and awards, including the Best Young Engineer Paper Award at the 29th ESA Workshop on Antennas in 2007, an ESA Teamwork Excellence Award in 2020, and several ESA Technical Improvement Awards. He served as the Chair of the 38th ESA Antenna workshop in 2017, and as the Co-Chair of the 2018 IET Loughborough Antennas and Propagation Conference in 2018. He is also serving as the Co-Vice Chair of the newly founded IEEE MTT-S Technical Committee 29 on Microwave Aerospace Systems. He has been a Board Member of the European School of Antennas and Propagation (ESoA) since January 2019 and is also serving as a Coordinator of the ESA/ESoA course on Antennas for Space Applications, for which he was voted best lecturer by the participants of the 2020 edition. He is the elected EurAAP Regional Delegate representing Benelux for the term 2021–2023. He is currently serving as an Associate Editor for the *IET Microwaves, Antennas and Propagation* and for IEEE TRANSACTIONS ON MICROWAVE THEORY AND TECHNIQUES, and as a Topic Editor for IEEE JOURNAL OF MICROWAVES.